

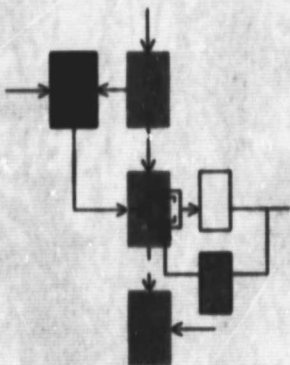
General Disclaimer

One or more of the Following Statements may affect this Document

- This document has been reproduced from the best copy furnished by the organizational source. It is being released in the interest of making available as much information as possible.
- This document may contain data, which exceeds the sheet parameters. It was furnished in this condition by the organizational source and is the best copy available.
- This document may contain tone-on-tone or color graphs, charts and/or pictures, which have been reproduced in black and white.
- This document is paginated as submitted by the original source.
- Portions of this document are not fully legible due to the historical nature of some of the material. However, it is the best reproduction available from the original submission.

September, 1968

REPORT ESL- FR-361
M.I.T. PROJECT DSR 76152
NASA Research Grant NSG-496 (Part)



INVESTIGATION OF COINCIDENT RADIO-FREQUENCY DRIVE FOR NDRO IN THIN-FILM MEMORIES

W. Stewart Nicol

FACILITY FORM 602	N 69-14766	(ACCESSION NUMBER)	(THRU)
	80	(PAGES)	1
	98747	(NASA GR OR TMX OR AD NUMBER)	08
			(CATEGORY)



Electronic Systems Laboratory

MASSACHUSETTS INSTITUTE OF TECHNOLOGY, CAMBRIDGE, MASSACHUSETTS 02139

Department of Electrical Engineering

September, 1968

Final Report ESL-FR-361

Copy 18

INVESTIGATION OF COINCIDENT RADIO-FREQUENCY DRIVE FOR
NONDESTRUCTIVE READOUT IN THIN-FILM MEMORIES

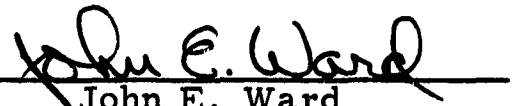
by

W. Stewart Nicol

The preparation and publication of this report, including a portion of the research on which it is based, was sponsored under a grant to the Electronic Systems Laboratory, Massachusetts Institute of Technology (MIT Project No. 76152). This grant is being administered as part of the National Aeronautics and Space Administration Research Grant No. NSG 496 (Part). The initial phases of the work were performed under contract AF-33(657)-11311 (MIT Project No. 79891), sponsored by the Air Force Avionics Laboratory, Wright-Patterson Air Force Base.

This report is published for information purposes only and does not represent recommendations or conclusions of the sponsoring agencies. Reproduction in whole or in part is permitted for any purpose of the United States Government.

Approved by


John E. Ward
Deputy Director

Electronic Systems Laboratory
Department of Electrical Engineering
Massachusetts Institute of Technology
Cambridge, Massachusetts 02139

PRECEDING PAGE BLANK NOT FILMED.

ABSTRACT

An investigation of the feasibility of applying radio-frequency drive techniques to a nondestructive readout (NDRO) thin magnetic film memory is described. The method was demonstrated as being very successful in obtaining coincident-frequency NDRO. Drive currents of 20 MHz and 40 MHz were used during readout, when it was observed that values for these currents as low as 30 mA peak-to-peak with 20-mil wide drive lines still gave discernible output signals.

Coincident radio-frequency writing was found to be possible only under critical phase and bias conditions, being limited by domain boundary creep and noncoherent magnetization rotation.

ACKNOWLEDGMENT

The author wishes to acknowledge Professors James G. Gottling and Alfred K. Susskind for the suggestion of and subsequent contributions to this investigation. He would also like to thank Dr. Haruhisa Ishida, University of Tokyo, for the computer simulation and his very valuable experimental work. Numerous helpful discussions with Thomas S. Crowther, Lincoln Laboratory, are also greatly appreciated.

From its inception in early 1964 until mid-1965, this work was supported by the U.S. Air Force Avionics Laboratory under Contract AF-33(657)-11311. The remainder of the active research effort which ended in late 1966, and the subsequent preparation of this report have been supported by NASA Grant NsG-496 (Part). The interest and support of these sponsors is gratefully acknowledged.

CONTENTS

	<u>page</u>	
CHAPTER I		INTRODUCTION
		1
A.		Summary
		1
B.		Motivation
		1
C.		Radio-Frequency Methods
		2
		1. Radio-Frequency Readout
		3
		2. Radio-Frequency Writing
		3
CHAPTER II		THEORETICAL STUDY OF THE NON-DESTRUCTIVE READOUT MODE
		7
A.		Single-Domain Model
		7
B.		Choice of Drive-Current Frequencies
		8
C.		Computer Simulation of the Readout
		11
		1. Drive-amplitude Dependence
		12
		2. Effect of a d-c Longitudinal Field, H_{L0}
		14
		3. Effect of Skew Angle, α
		14
		4. Effect of a d-c Transverse Field, H_{T0}
		14
		5. Effect of a Phase Difference, β
		14
CHAPTER III		EXPERIMENTAL OBSERVATIONS OF THE NDRO MODE
		16
A.		Memory Test Apparatus
		16
B.		Characteristics of the Magnetic Films
		19
		1. Measurements at 1 KHz
		19
		2. Evaporation of Thin Magnetic Films
		19
		3. Bitter Pattern Observations
		21
C.		Observations of Film Behavior in the NDRO Mode
		21
		1. Film Output Voltage at 60 MHz for Small R-F Signal Drive
		22
		2. Disturb Values of Radio-Frequency Drive Currents
		24

CONTENTS (Contd.)

	3. The Influence of a d-c Bias Field along the Easy Axis	<u>page</u>	24
	4. Phase Effects of the NDRO Drive Currents		26
	5. Effect of Film Parameters		26
	6. Comparison of Continuous Sheet, Photo-etched, and Mask-evaporated Films		26
	7. Comparison of Transmission Line Configurations		27
CHAPTER IV	THEORETICAL BASIS FOR COINCIDENT PULSE AND COINCIDENT RADIO-FREQUENCY WRITE SCHEMES		29
A.	Coincident Pulse Writing		30
B.	Coincident Radio-Frequency Writing		32
	1. Even-Mode Writing		32
	2. Odd-Mode Writing		33
	3. Comparison of Even- and Odd-Mode Writing		33
CHAPTER V	EXPERIMENTAL OBSERVATIONS OF COINCIDENT PULSE AND COINCIDENT RADIO-FREQUENCY WRITE SCHEMES		35
A.	Coincident Pulse-Write Experiments		35
B.	Coincident Radio-Frequency Writing		40
C.	Discussion of Coincident Radio-Frequency Writing		41
CHAPTER VI	CONCLUSIONS		45
A.	Coincident Radio-Frequency NDRO		45
B.	Coincident Radio-Frequency Writing		45
C.	Suggestions for Future Investigations		46
APPENDIX A	FLOW CHART OF THE COMPUTER PROGRAM TO FIND θ FROM A GIVEN H_L AND H_T		47
APPENDIX B	SUMMARY OF PARAMETERS OF FILMS EXAMINED		49

CONTENTS (Contd.)

APPENDIX C	MAGNETIC FIELD OF SQUARE HELMHOLTZ COILS	<u>page</u>	56
APPENDIX D	SELECTION RATIO FOR COINCIDENT-CURRENT WRITING		60
1.	Maximum Value for the Selection Ratio		61
2.	Values of Word Currents Giving the Maximum Selection Ratio		61
APPENDIX E	FACTORS INFLUENCING SWITCHING OF IDEAL FILMS		64
1.	Nonuniformity of the Applied Fields		64
2.	Demagnetizing Fields		67
3.	Eddy Current		72
APPENDIX F	RADIO-FREQUENCY DRIVE-LINE AND SENSE CIRCUITRY		74
REFERENCES			76

LIST OF FIGURES

	<u>page</u>
1. Memory Cell and Organization of a Coincident-Frequency Memory	4
2. Critical Switching Curve for a Uniaxial Film	6
3. Theoretical Variation of Output Amplitude with Transverse Drive Field	13
4. Theoretical Variation of Output Amplitude with d-c Bias Along the Easy Axis	13
5. Theoretical Effect of a Transverse d-c Field	15
6. Total r-f Drive Current Function, $\cos\omega t + \cos 2\omega t$	15
7. Memory Test Apparatus	17
8. Variation of Sense Amplifier Output Voltage with Transverse r-f Drive Current Amplitudes in the NDRO Mode.	23
9. Variation of Sense Amplifier Output Voltages with Film Thickness for Various NDRO Drive Current Amplitudes	23
10. Nondestructive Readout Signals	22
11. Transmission Line Configurations	27
12. Schemes for Coincident-Pulse Writing and Coincident-Frequency Writing	31
13. Coincident Pulse Writing. Film No. 327	37
14. Coincident Pulse Writing. Film No. 332	37
15. Coincident Pulse Writing. Film No. 210P6B	38
16. Coincident Pulse Writing. Film No. 337	38
17. Switching Field Loci for Coincident-Frequency Writing and Non-writing. Film No. 328	42
18. Switching Field Loci for Coincident-Frequency Writing. Film No. 328	43
19. Flow Chart of the Computer Program to Find θ from a Given H_L and H_T	48

LIST OF FIGURES (Contd.)

20.	Field Diagram of Single Turn Square Coil	<u>page</u>	58
21.	Distances Used in Calculating Square Helmholtz Coil Separation		58
22.	Word Drive Currents Used in Obtaining the Selection Ratio		60
23.	Model for Magnetization and Demagnetizing Field Distributions		71
24.	Eddy Current Pattern in a Conductor		72
25.	Radio-Frequency Drive and Sense Circuitry Block Diagram		75

CHAPTER I

INTRODUCTION

A. SUMMARY

This report describes an investigation made to determine the feasibility of applying a radio-frequency drive method for reading and writing of information in a thin magnetic film memory. The method was demonstrated as being very successful in obtaining coincident-frequency nondestructive readout (NDRO). Row and column drive currents of 20 MHz and 40 MHz, respectively, were used during readout, and it was observed that with 20-mil wide drive lines the values of these currents could be as low as 30 mA peak-to-peak and still give discernible output signals.

Coincident r-f writing, on the other hand, proved to be much more difficult, being limited by the problems of domain boundary creep and noncoherent magnetization rotation. Coincident r-f writing was only obtained with difficulty, having the additional requirements of a d-c biasing field and critical relative phase adjustments between the drive currents.

B. MOTIVATION

This research was undertaken with the main objective of investigating the applicability of r-f techniques towards obtaining a high-density, thin magnetic film memory requiring a minimum of selection circuitry, and nondestructive reading of information.

The concept explored uses conventional coincident-current organization, similar to that in conventional memories based on magnetic cores. When there are N^2 words in a coincident-current memory, all the words are arranged in a two-dimensional fashion in the form of an $N \times N$ matrix. The selection of a particular word is accomplished by choosing the word at the intersection of one of N rows of words and one of N columns of words. Thus the number of necessary selection lines is $2N$. By contrast, all N^2 words are arranged in a one-dimensional array in a word-organized memory, and the number

of necessary word selection lines is N^2 in such a memory with equal capacity.

Memory operation can be classified by the manner in which stored information is interrogated: destructive readout (DRO) or nondestructive readout (NDRO). NDRO memory operation can be advantageous because there is no requirement to rewrite the information following readout if it is to be preserved for future reference.

C. RADIO-FREQUENCY METHODS

The application of r-f drive currents to magnetic memories, either ferrite core or thin ferromagnetic film, has been described by several authors. B. Widrow^{1*} has applied the method to coincident-current selection in a ferrite core memory. J. H. Hoper² has described an application to a thin-film memory. The drive frequency used was 1 MHz. For nondestructive readout a single frequency was applied to the transverse axis. The direction of magnetization was then sensed from the phase of the first or second harmonic component of the time rate of change of the easy-axis magnetization. Switching was accomplished by having orthogonal drive fields along the longitudinal and transverse axes. C. J. Bader and D. M. Ellis have described³ an application of r-f fields in an instrument for determining the direction of the magnetization in small regions of a magnetic film. The instrument uses a crossed-wire probe; the wires are orthogonal and driven by 8-MHz and 11-MHz signals. The sum frequency of 19 MHz is detected by a tuned sense amplifier. H. W. Fuller, et al,⁴ have described an experimental memory system employing sum-frequency detection, and using etched permalloy-sheet toroids. The readout drive scheme uses orthogonal driving fields. A further description of techniques applied to permalloy toroids has been given by R. J. Webber, et al.⁵

More recently H. H. Zappe⁶ has applied an r-f technique for measuring thin-film parameters. This uses two orthogonal loops wound around a nonconductive probe. One loop carries a sinusoidal high-frequency current which causes a small local oscillation of the

*Superscripts refer to numbered items in the list of References.

magnetization when the probe is held near the surface of the film. The second harmonic component of the voltage induced in the orthogonal loop is used to measure the film parameters. The basic frequency is 10 MHz.

The techniques described in this report have used orthogonal drive fields at the higher frequencies of 20 MHz and 40 MHz.

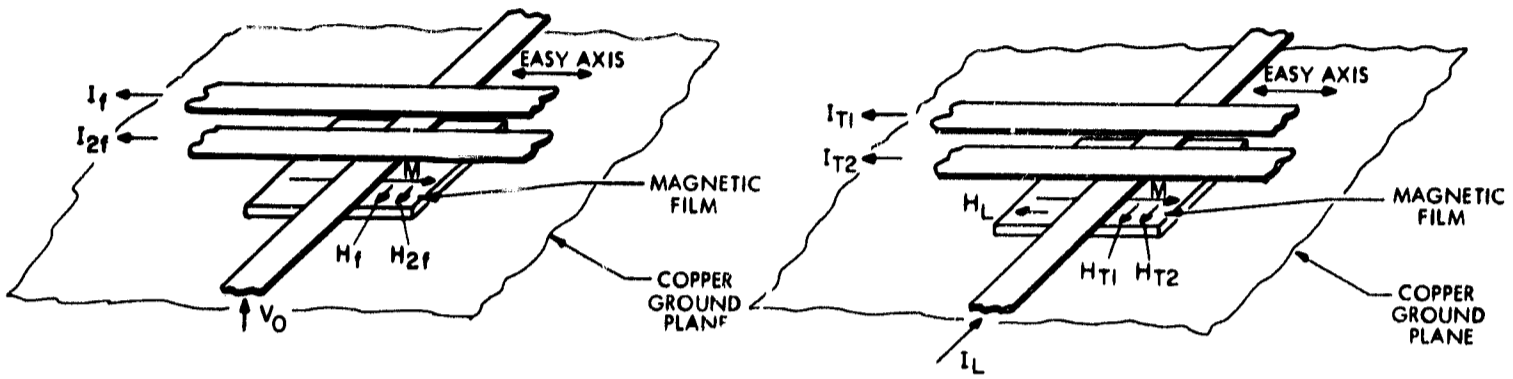
1. Radio-Frequency Readout

The memory concept which we have investigated is shown in Fig. 1. Figures 1a and b show the basic r-f readout and write drive schemes, respectively, for a selected memory cell. Figure 1c illustrates the memory organization for the case of a nine-word array with three bits per word, indicated by a rectangle.

During readout, a keyed current of frequency f_1 drives a selected row, and a keyed current of frequency f_2 drives a selected column. Only the film elements at the intersection of the selected column drive-line and the selected row drive-line are energized by fields of both frequencies f_1 and f_2 , and, since their response is nonlinear, they act as nonlinear mixing elements to produce frequency components at d-c, $2f_1$, (f_2-f_1) , $2f_2$, (f_1+f_2) , etc. The output phase of the sum-frequency component (f_1+f_2) is 0 or π , depending on the direction of initial magnetization of the selected film element. By filtering the sense-line output, this sum-frequency component can be detected. This particular r-f method was confirmed by experiment as a successful means of readout.

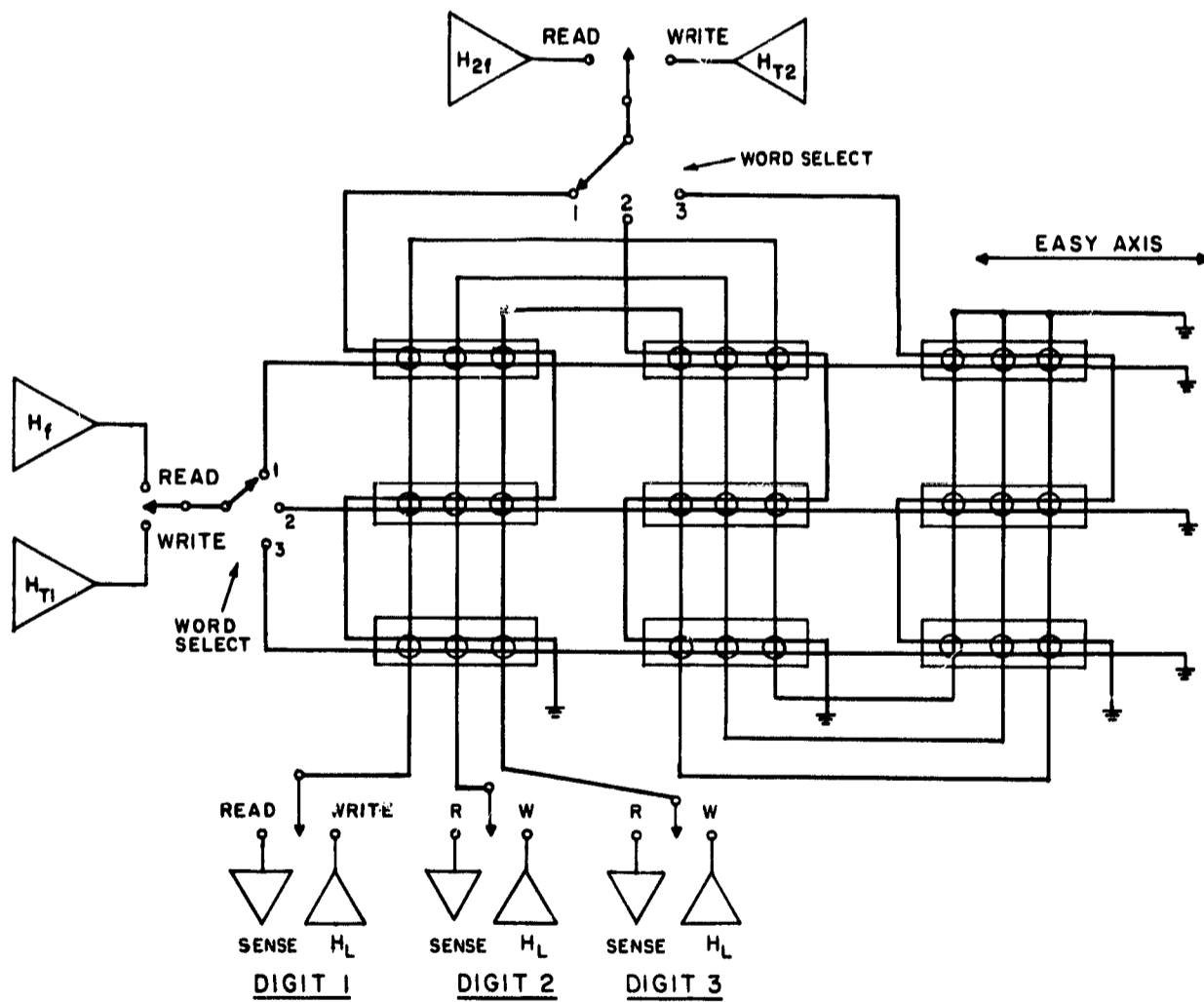
2. Radio-Frequency Writing

Two modes of writing were examined: conventional coincident pulse and coincident radio-frequency. Proper coincident pulse writing depends on assuring that for H_{T1} and H_{T2} sufficiently applied along the transverse (hard-axis) direction, together with H_L applied along the longitudinal (easy-axis) direction, switching of the magnetization can take place, whereas no switching must occur for the combination of H_{T1} and $\pm H_L$, or of H_{T2} and $\pm H_L$ applied separately. These criteria place stringent requirements on the magnetic film elements. In the Stoner-Wohlfarth, single-domain model, switching occurs by



(a) READ-OUT CURRENTS FOR FULLY SELECTED MEMORY CELL

(b) WRITE CURRENTS FOR FULLY SELECTED MEMORY CELL



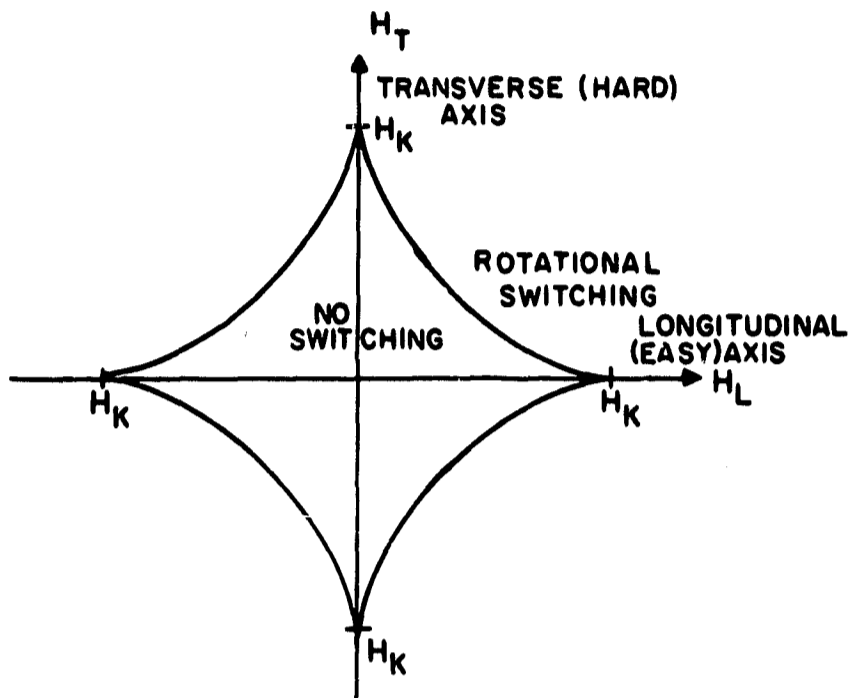
(c) ORGANIZATION OF A NINE-WORD COINCIDENT FREQUENCY MEMORY HAVING 3 BITS PER WORD

Fig. 1 Memory Cells and Organization of a Coincident-Frequency Memory

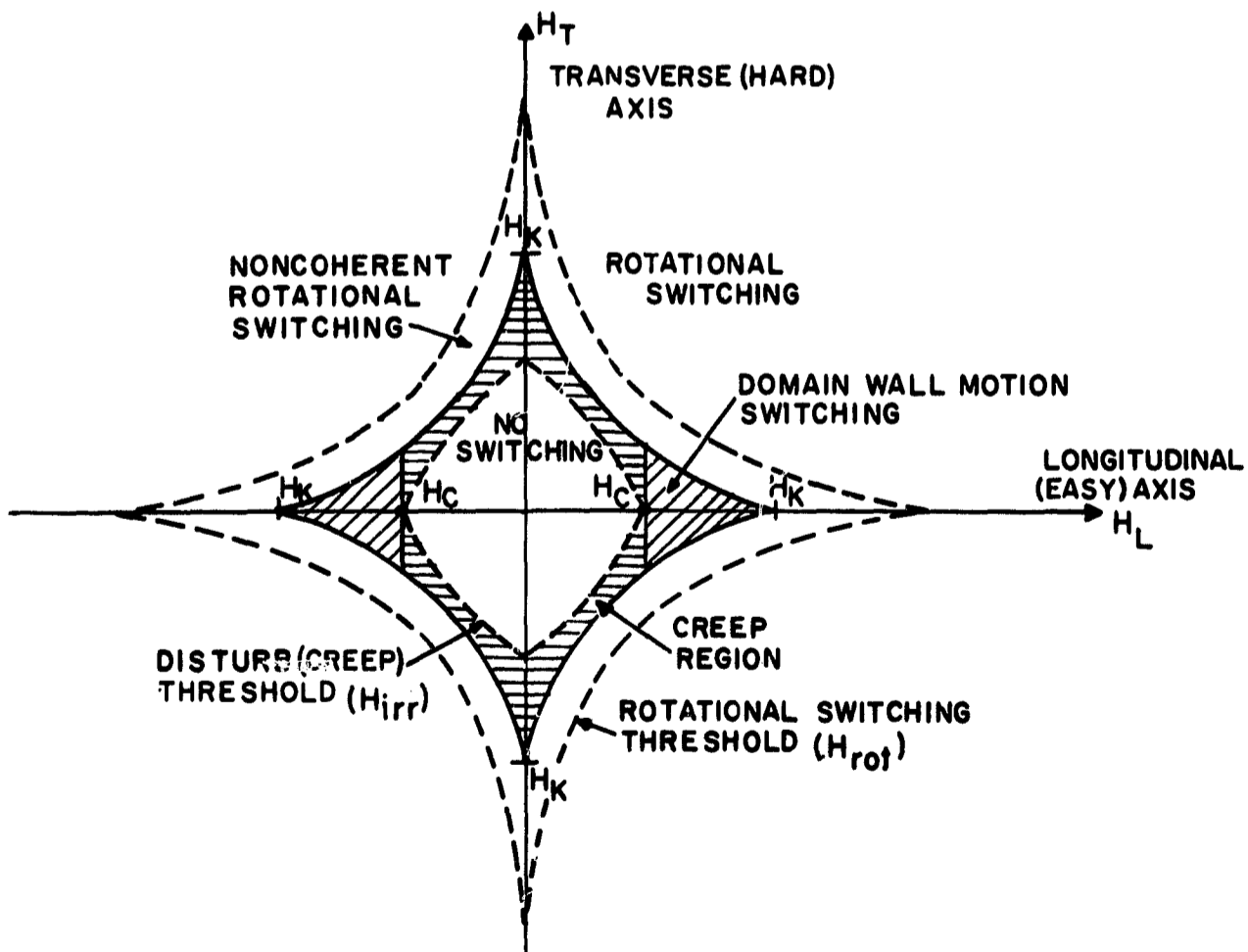
coherent rotation of the magnetization as indicated in Fig. 2a. For practical film elements, however, as in Fig. 2b, the regions of non-coherent rotational switching, domain wall motion, and creep switching are severe limitations for coincident-current operation.

A coincident-frequency write scheme was attempted in the hope that the creep threshold, H_{irr} , might be larger for sinusoidal fields rather than for pulsed fields along both transverse and longitudinal axes. This hope is based on the observation that the average displacement of the magnetization under sinusoidal excitation in half-selected memory cells is zero, and the fact that in pulse writing the application of bipolar pulses does decrease creeping.

It was demonstrated experimentally that coincident r-f writing was possible, using transverse drive currents of 20 MHz and 40 MHz and a longitudinal drive current of 20 MHz. However, whether or not writing occurred depended critically on the relative phases of the longitudinal and transverse drive currents. Also the values of phase angle under coincident operation, however, did not agree with those expected theoretically and from the results it was concluded that the writing observed was essentially a creep-mode.



(a) Stoner-Wohlfarth Model



(b) Practical Model

Fig. 2 Critical Switching Curve for a Uniaxial Film

CHAPTER II

THEORETICAL STUDY OF THE NONDESTRUCTIVE READOUT MODE

In this chapter we describe the theoretical basis for the non-destructive readout (NDRO) mode. The single-domain model is treated first, since, as our subsequent experiments have shown, it provides an adequate description of small-signal operation of the NDRO mode. Second, a simplified analysis of the small-signal, single-domain model, leading to the choice of drive-current frequencies, is considered. Finally, because of the nonlinear form of the single-domain equations for large amplitudes, the influence of drive-amplitude, d-c bias fields along the transverse and longitudinal axes, and of skew angle on the NDRO output, is treated in a more elaborate analysis using an IBM 7094 computer program.

A. SINGLE-DOMAIN MODEL

It is customary to start a discussion on thin-magnetic films with the assumption that the films behave essentially as a single domain. In reality, however, this is a very gross approximation, valid only for small-signal operation. For large-signal operation involving switching, the model breaks down even as an approximation, because of its lack of time dependency and its omission of wall motion, incoherent rotation, creep, etc. This implies that, whereas it may be impossible to apply the single-domain model in devising a scheme for writing, which involves switching, it may be perfectly applicable in describing small-signal NDRO behavior. This is borne out by our experiments.

According to the single-domain model,⁷ the angle, θ , between the direction of the magnetization, M_S , and the easy axis is determined from the energy expression:

$$E = \frac{H_K M_S}{2} \sin^2 \theta - H_L M_S \cos \theta - H_T M_S \sin \theta \quad (1)$$

by the minimum energy condition:

$$H_K \sin \theta \cos \theta + H_L \sin \theta - H_T \cos \theta = 0 \quad (2)$$

with the stability condition

$$H_K (\cos^2 \theta - \sin^2 \theta) + H_L \cos \theta + H_T \sin \theta \geq 0 \quad (3)$$

M_S is the saturation magnetization, H_K is the anisotropy field, and $0 \leq \theta \leq 360^\circ$. H_L is the longitudinal (easy-axis) field and H_T is the transverse (hard-axis) field. The easy-axis component, M_L , of the magnetization is determined by θ ,

$$M_L = M_S \cos \theta \quad (4)$$

Considering the case where $H_L = 0$, $\theta \neq 90^\circ$, $\theta \neq 270^\circ$, and $H_T \leq H_K$, from Eq. 2, $H_T = H_K \sin \theta$, which also satisfies Eq. 3. Substituting $\sin \theta = H_T/H_K$ into Eq. 4 gives:

$$M_L = \pm M_S \sqrt{1 - \left(\frac{H_T}{H_K}\right)^2} \quad (5)$$

When H_T is small compared to H_K ,

$$M_L \approx \pm M_S \left[1 - \frac{1}{2} \left(\frac{H_T}{H_K}\right)^2 \right] \quad (6)$$

This expression is used later in analyzing the r-f nondestructive read-out method.

B. CHOICE OF DRIVE-CURRENT FREQUENCIES

We first show that the sense output voltage is related to the drive-current frequencies, and estimate this voltage for a particular choice of frequency. The coincident-current NDRO method investigated used a current of frequency ω_1 driving a selected word row and a current of frequency ω_2 driving a selected word column. As shown in Fig. 1c, only memory cells directly under both the select row and column drive lines are energized by transverse fields of both frequencies ω_1 and ω_2 . Each of these cells acts as a nonlinear mixing element to produce a sum-frequency component ($\omega_1 + \omega_2$). The phase of this component is 0 or π depending on the polarity of magnetization in each cell. It is detected as the output signal from the cell through a sense line placed in the transverse axis direction.

Since the sensed signal is the rate of change of the easy-axis flux, its overall characteristics may be analyzed using the single-domain model. Suppose that the total transverse drive field is of the form

$$H_T = H_{T1} \cos \omega_1 t + H_{T2} \cos \omega_2 t \quad (7)$$

Substituting in Eq. 6 gives

$$M_L = \pm M_S \left[1 - \frac{H_{T1}^2}{2H_K^2} \cos^2 \omega_1 t - \frac{H_{T1} H_{T2}}{H_K^2} \cos \omega_1 t \cos \omega_2 t - \frac{H_{T2}^2}{2H_K^2} \cos^2 \omega_2 t \right] \quad (8)$$

that is,

$$M_L = \pm M_S \left[1 - \frac{H_{T1}^2 + H_{T2}^2}{4H_K^2} - \frac{H_{T1}^2}{4H_K^2} \cos 2\omega_1 t - \frac{H_{T1} H_{T2}}{2H_K^2} \cos(\omega_1 + \omega_2)t - \frac{H_{T1} H_{T2}}{2H_K^2} \cos(\omega_1 - \omega_2)t - \frac{H_{T2}^2}{4H_K^2} \cos 2\omega_2 t \right] \quad (9)$$

The output components producing the largest rates of flux change are the sum-frequency $(\omega_1 + \omega_2)$ and difference-frequency $(\omega_1 - \omega_2)$ components. The sum component is in fact:

$$M_{L'} = \pm M_S \frac{H_{T1} H_{T2}}{2H_K^2} \cos(\omega_1 + \omega_2)t \quad (10)$$

The corresponding output voltage V_L is

$$V_L = \pm M_S \ell d(\omega_1 + \omega_2) \frac{H_{T1} H_{T2}}{H_K^2} \sin(\omega_1 + \omega_2)t \quad (11)$$

where d is film thickness and ℓ is the effective width of flux change.

The magnitude of V_L can be estimated assuming the following conditions:

$$d = 500\text{\AA} = 5 \times 10^{-8} \text{ m.}$$

$$l = 40 \text{ mil} = 1 \text{ mm} = 10^{-3} \text{ m.}$$

$$M_S = 10^4 \text{ gauss} = 1 \text{ weber/m}^2$$

$$H_{T1}/H_K = H_{T2}/H_K = 0.25$$

$$(\omega_1 + \omega_2) = 2\pi \times 60 \times 10^6 \text{ (60 MHz)}$$

The peak amplitude of V_L is approximately 1 millivolt. Therefore, if a sense amplifier with a gain of 2000 is available, an output voltage of 4 volts peak-to-peak may be expected. It is noted that the output amplitude is proportional to the sum-frequency so that increasing the drive frequency increases the output, limited only by magnetic resonance.

Many choices are conceivable in selecting the two frequencies ω_1 and ω_2 . Since the output contains components of $2\omega_1$, $2\omega_2$, $(\omega_2 - \omega_1)$ and possibly ω_1 and ω_2 occurring as drive-to-sense-line coupling noise, it might be argued that ω_2 should differ from $2\omega_1$ or $(\omega_2 - \omega_1)$. However, from considerations of faster operating speed, ease of locking phases, and compatibility with the r-f writing scheme, (Chapter IV, Section 3), a choice of $\omega_2 = 2\omega_1$ was made. Accordingly, the total ω_1 noise component, being the sum of ω_1 and $(\omega_2 - \omega_1)$ noise components, and the total ω_2 noise component, being the sum of ω_2 and $2\omega_1$ noise components, may be larger, but they can easily be eliminated by tuned filtering.

In the actual memory, the two r-f drive currents have to be keyed or modulated by square waves. Assuming n-cycle readout and a 50 percent duty cycle, the maximum keying frequency is $\omega_1/2n$. The sense amplifier tuned to the center frequency $\omega_1 + \omega_2 = 3\omega_1$ should have a bandwidth $\Delta\omega = 4\pi/t_p$, where t_p is the square pulse duration time. Thus, since $\omega_1 = 2\pi n/t_p$, $\Delta\omega = 2\omega_1/n$.

The frequencies chosen for the experimental study of the NDRO mode were $f_1 = \omega_1/2\pi = 20 \text{ MHz}$, and $f_2 = \omega_2/2\pi = 40 \text{ MHz}$. The sense amplifier was therefore tuned to a frequency of 60 MHz.

C. COMPUTER SIMULATION OF THE READOUT

A more elaborate analysis of the r-f readout characteristics was made by programming the IBM 7094 at the MIT Computation Center. The objective was to find the effects of easy-axis skew angle α , transverse drive amplitudes H_f and H_{2f} , transverse and longitudinal d-c bias fields H_{T0} and H_{L0} , and phase difference β between the two transverse drive fields. The basis of the analysis is the single-domain model, but with no restriction on the amplitude of the angle θ .

The drive fields are assumed to be of the form:

$$H_T = [H_f \cos \omega t + H_{2f} \cos(2\omega t + \beta) + H_{T0}] \cos \alpha - H_{L0} \sin \alpha \quad (12a)$$

$$H_L = [H_f \cos \omega t + H_{2f} \cos(2\omega t + \beta) + H_{T0}] \sin \alpha + H_{L0} \cos \alpha \quad (12b)$$

in which it is to be understood that the total transverse and longitudinal drive fields, H_T and H_L , are normalized with respect to H_K . The angle θ between the magnetization vector and the easy axis is determined by Eq. 2 for a given set of H_T and H_L . The amplitudes of the 3ω sine and cosine components of the output voltage, omitting constant multipliers, are given by:

$$V_s(3\omega) = \left[\int_0^T \cos \theta \cdot \cos 3\omega t \, dt \right] \cos \alpha \quad (13a)$$

$$V_c(3\omega) = \left[\int_0^T \cos \theta \cdot \sin 3\omega t \, dt \right] \cos \alpha \quad (T = \frac{2\pi}{\omega}) \quad (13b)$$

Note that it is not necessary to take the time derivative of $M = M_s \cos \theta$ to get the above Fourier components, since

$$\begin{aligned} \int_0^T \frac{dM}{dt} \cos 3\omega t \, dt &= M \cos 3\omega t \Big|_0^T + 3\omega \int_0^T M \sin 3\omega t \, dt \\ &= 3\omega \int_0^T M \sin 3\omega t \, dt \end{aligned} \quad (14a)$$

Similarly

$$\int_0^T \frac{dM}{dt} \sin 3\omega t dt = 3\omega \int_0^T M \cos 3\omega t dt \quad (14b)$$

Note also that $V_c(3\omega) = 0$ as long as $\beta = 0$, because Eq. 3 is then an even function of time, t .

The amplitude $A(3\omega)$ of the total output is calculated as

$$A(3\omega) = \sqrt{V_c(3\omega)^2 + V_s(3\omega)^2} \quad (15a)$$

and its phase ϕ is

$$\phi = \tan^{-1}[V_s(3\omega)/V_c(3\omega)] \quad (15b)$$

The first part of the computer program evaluates H_T and H_L at a given instant of time for a given set of H_f , H_{2f} , α , β , H_{T0} and H_{L0} . It is important to note that the drive fields, H_f , H_{2f} , etc., are normalized with respect to H_K . The second part determines θ satisfying $f(\theta) = 0$ and $f'(\theta) \geq 0$ for such H_T and H_L , where $f(\theta)$ is the left-hand side of Eq. 2. The flow chart of this part of the program is shown in Appendix A. The third part is the numerical integration for $V_s(3\omega)$, $V_c(3\omega)$, $A(3\omega)$ and ϕ . The interval $[0, T]$ is divided into eight equal sections and the Gauss 7-point formula is used in each section.

There are six parameters H_f , H_{2f} , H_{T0} , H_{L0} , α and β , involved in the calculation. Many combinations of these parameters were used to observe their effects on the output.

The following is a summary of the computer analysis.

1. Drive-amplitude Dependence

Figure 3 shows the drive-amplitude dependence of the output signal with $\alpha = \beta = H_{T0} = 0$. $H_{L0} = 0.01$. When one drive amplitude is fixed, a maximum output results at $H_f + H_{2f}$ slightly larger than 1. When both H_f and H_{2f} are increased, the output continues to increase and reaches a maximum at about $H_f + H_{2f} = 2.3$ where the negative peak of the combined drive reaches -1 .

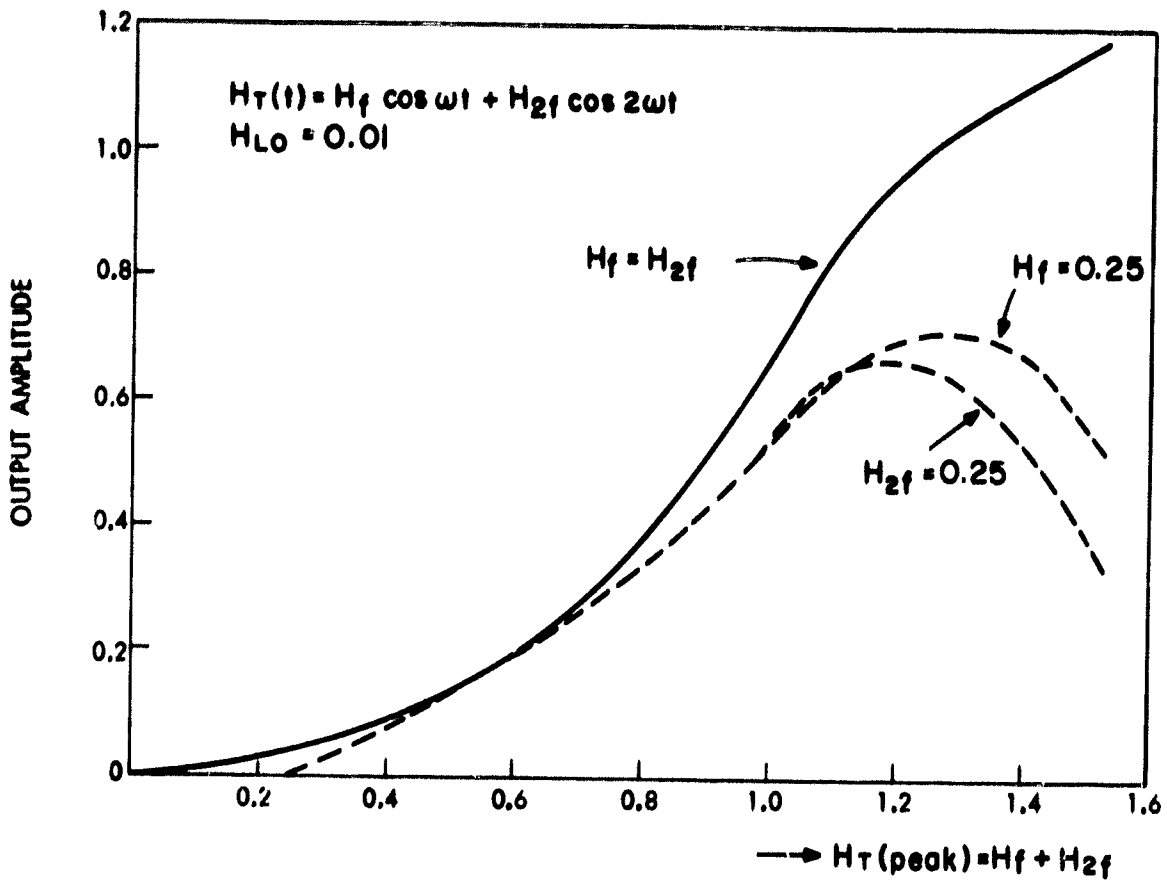


Fig. 3 Theoretical Variation of Output Amplitude with Transverse Drive Field

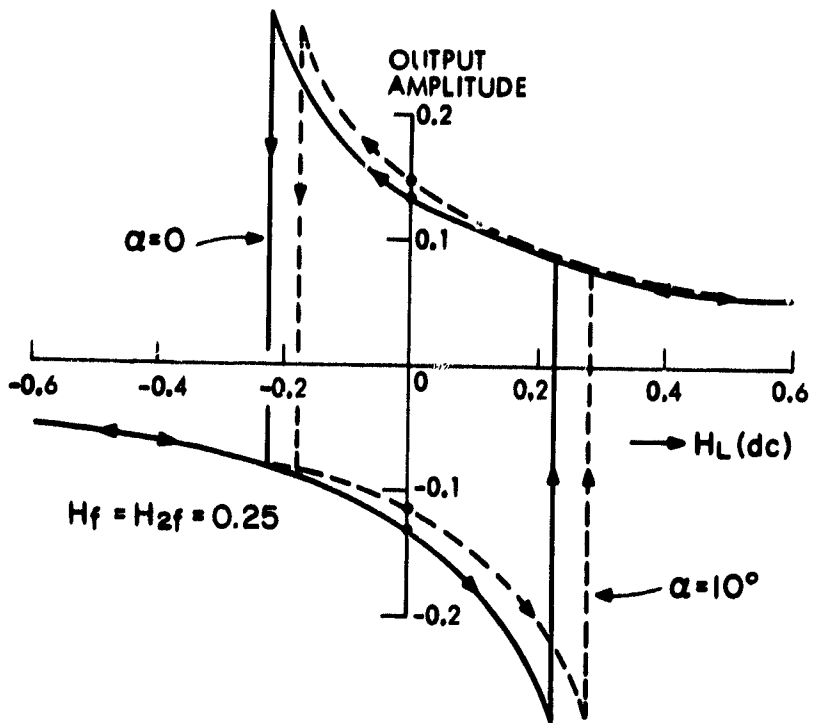


Fig. 4 Theoretical Variation of Output Amplitude with d-c Bias Along the Easy Axis

2. Effect of a d-c Longitudinal Field, H_{L0}

Figure 4 shows the d-c longitudinal field dependence of the output when there is no skew and also when there is a 10° skew angle ($\alpha = 10^\circ$, $H_f = H_{2f} = 0.25$, $\beta = 0$, $H_{T0} = 0$).

3. Effect of Skew Angle, α

When there is skew, the binary outputs are not symmetric in amplitude, as shown in Fig. 4. Asymmetry then also arises in switching thresholds.

4. Effect of a d-c Transverse Field, H_{T0}

This effect is shown in Fig. 5. It is to be noted that the r-f field is not symmetric in amplitude in the positive and negative directions. Since

$$H_T = H_f \cos \omega t + H_{2f} \cos 2\omega t$$

there are three kinds of peaks in H_T determined by

$$\frac{dH_T}{dt} = -\omega \sin \omega t (H_f + 4H_{2f} \cos \omega t) = 0$$

That is, a positive peak = $H_f + H_{2f}$ when $\omega t = 0$

a middle peak = $-H_f + H_{2f}$ when $\omega t = \pi$

a negative peak = $\frac{-H_f^2}{8H_{2f}} - H_{2f}$ when $\cos \omega t = \frac{-H_f}{4H_{2f}}$

The time variation of H_T , for the case of $H_f = H_{2f}$, is shown in Fig. 6. The presence of a d-c field, H_{T0} , tends to increase the output. The maxima then occur at approximately $H_f + H_{2f} + H_{T0} = 1.1$ and at

$$\frac{-H_f^2}{8H_{2f}} - H_{2f} + H_{T0} = -1.1$$

5. Effect of a Phase Difference, β

Under a typical condition ($H_f = H_{2f} = 0.25$, $\alpha = H_{T0} = H_{L0} = 0$), the presence of β merely introduces a phase shift in the output and there is no change in the total amplitude, $A(3\omega)$.

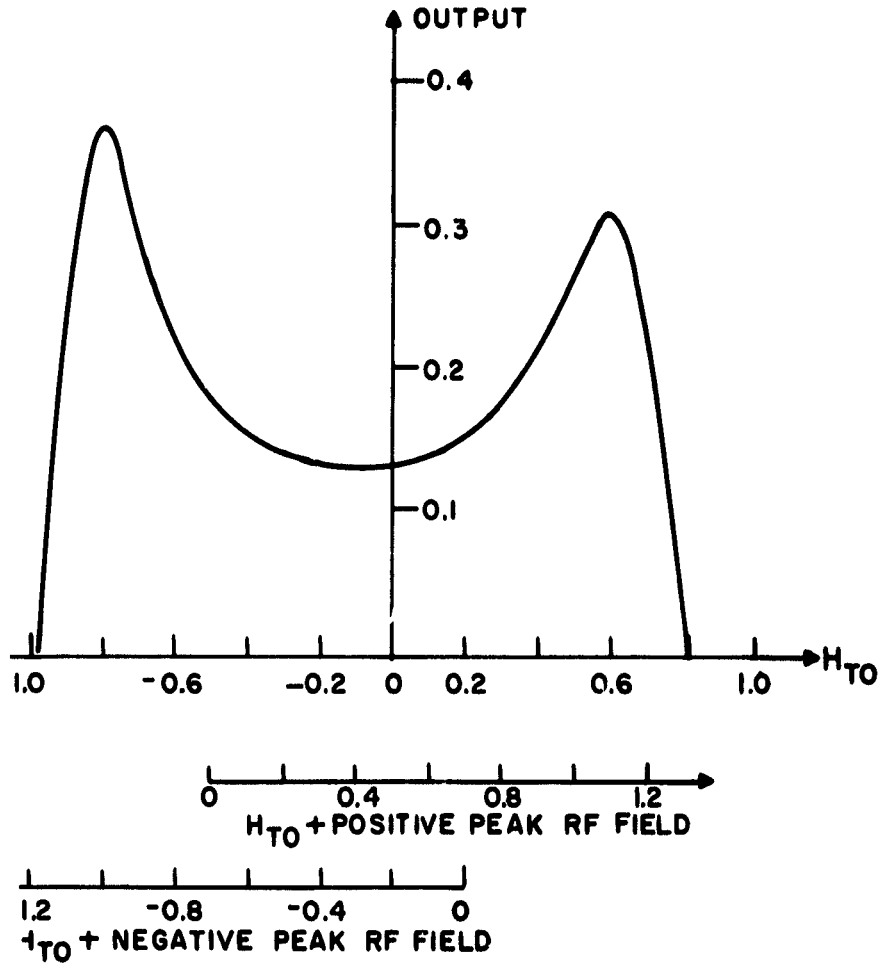


Fig. 5 Theoretical Effect of a Transverse d-c Field

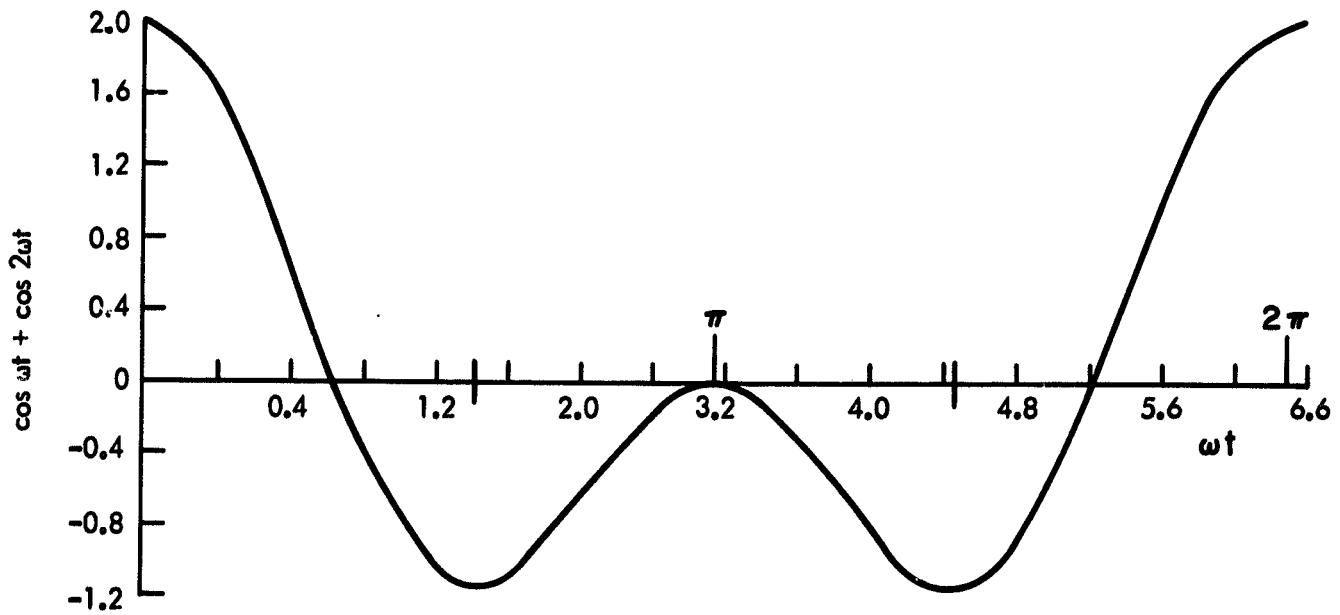


Fig. 6 Total r-f Drive Current Function, $\cos \omega t + \cos 2\omega t$

CHAPTER III

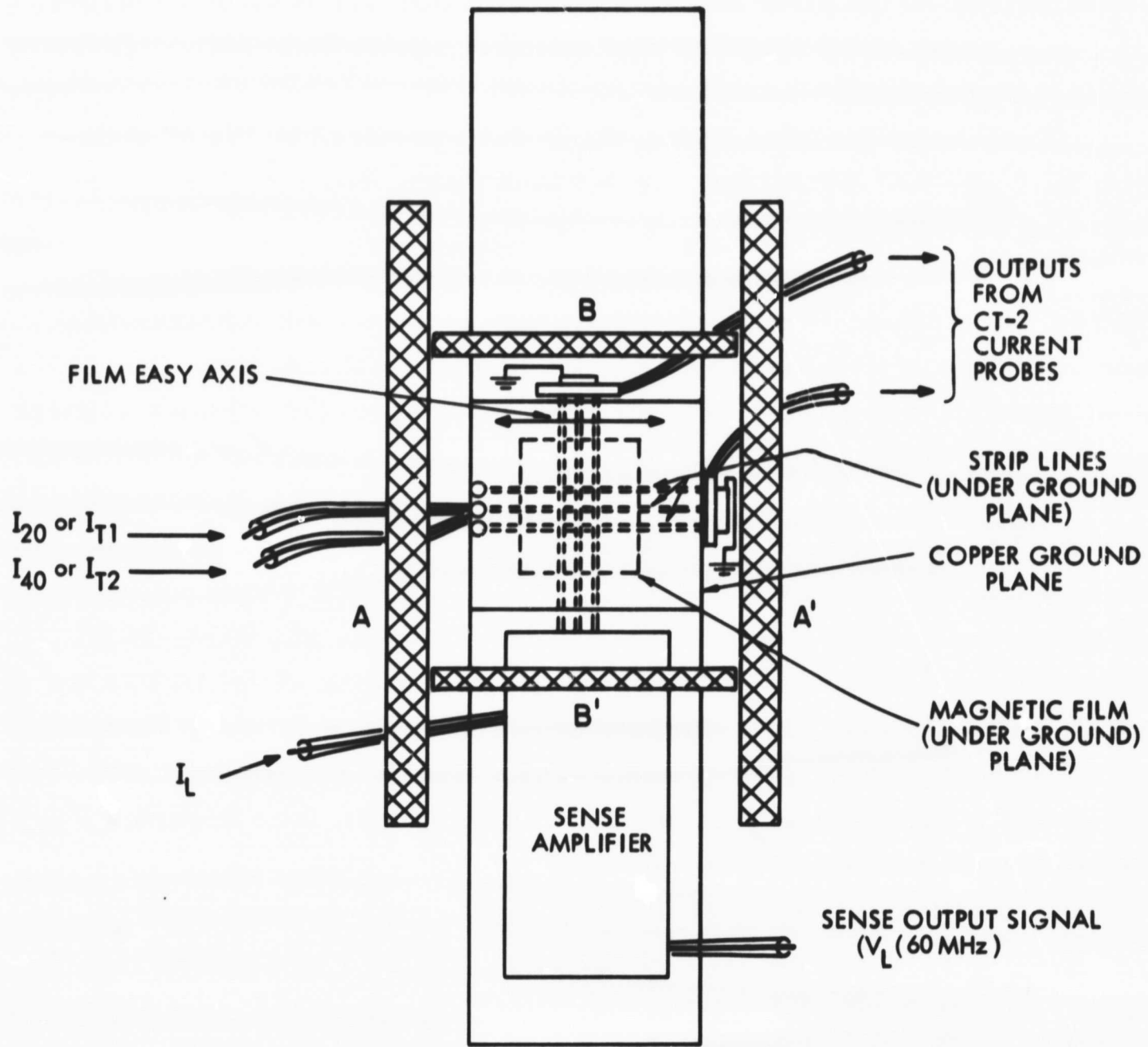
EXPERIMENTAL OBSERVATIONS OF THE NDRO MODE

The simplified analysis and computer solution of the NDRO mode are based on single domain theory. Besides providing the verification of this theory for small signals, an experimental investigation was then required to examine the following aspects of the NDRO mode:

1. The film output voltage of the sum-frequency (60 MHz) component for small r-f drive signals. From this, and a comparison with theory, an estimate of the total amount of magnetic flux being driven by the readout signals can be found.
2. The variation of sense output with r-f drive signals up to disturb values of drive field.
3. The influence of an external d-c bias field, H_{L0} , along the film easy axis. This is an important factor as it determines how important it is to apply a field cancelling the earth's magnetic field.
4. Whether there are, in practice, any relative phase effects of the r-f drive currents.
5. The effect of film parameters such as dispersion angle, α_q , wall motion coercive field, H_C , etc.
6. The relative merits of continuous sheet, etched, and mask evaporated magnetic films.
7. A comparison of various ways of coupling the r-f drive fields with the films. This is extremely important, since it includes an investigation of possible noise coupling between drive and sense lines, especially coupling introduced through the ground plane.

A. MEMORY TEST APPARATUS

The apparatus for investigating the feasibility of both the readout and the write modes is shown in Fig. 7. The two, circular, Helmholtz pairs AA' and BB' provide both cancellation of the horizontal component of the earth's magnetic field and d-c bias fields. A third pair of square Helmholtz coils (not indicated) were used initially to cancel the vertical component of the earth's field. It was found much easier to adjust the cancelling currents to obtain a completely field-free region, than to cancel the horizontal field component only. Obtaining a field-free region



8" DIAM. HELMHOLTZ COILS, AA', APPLY H_{LO}
4" DIAM. HELMHOLTZ COILS, BB', APPLY H_{TO}

Fig. 7 Memory Test Apparatus

using a Bell Model 240 Gaussmeter did not require accurate alignment of the axis of the Gaussmeter probe. After this adjustment had been made, the vertical cancellation was omitted, since the demagnetizing fields normal to the plane of a thin magnetic film are very much larger. The calculation of the optimum separation of square Helmholtz coils is given in Appendix C.

Easy-axis, d-c bias fields, H_{L0} , were provided by the 8" diameter coil pair AA' and transverse d-c bias fields, H_{T0} , by the 4" diameter coil pair BB'.

Pulse and r-f fields were applied by drive currents through strip transmission lines. The ground plane for one drive-line configuration consisted of a 1/4" thick copper block; in another drive line configuration, one side of a copper-clad epoxy sheet (1/16" thick copper) was used as the ground plane. The strip transmission lines were either 40-mil or 20-mil wide, etched from double, copper-clad, 2-mil epoxy board. The thickness of the lines was 1.4 mil (1-ounce copper), and their length was 3". Where necessary, half-mil thick mylar was used to separate overlying lines. Amphenol subminiature RG/U174, 50 Ω , coaxial cable and connectors were used to connect the strip lines to the r-f drive amplifiers. The currents were measured by placing Tektronix CT-2 current probes in the grounded end of each strip line.

The r-f drive circuitry was quite conventional, (see Appendix F), deriving the fundamental frequency and reference phase from a 10-MHz Colpitts oscillator. This signal passed through a frequency doubler and quadrupler to provide f_1 and f_2 . The relative phase adjustment of f_1 and f_2 was made by squaring and differentiating the 10-MHz signal and then feeding this differentiated signal into a Schmitt trigger, whose pulse on-time was variable. The differentiated trailing edge of this pulse controlled a frequency doubler having a 20-MHz (f_1) output.

The 60-MHz sense-amplifier consisted of a band-pass filter followed by several tuned collector stages.

For pulse-writing, synchronized EH132A and EH138 pulse generators were used. Both single pulse and pulse-train outputs were used.

The magnetic film substrates were 40-mil thick, 1.6" square glass, (American Saint Gobain, micro-lustraglass which is a

fire-polished, drawn glass). The drive-line to ground-plane separation was, therefore, at least 40 mil. A few later experiments were made with 9-mil thick glass substrates.

B. CHARACTERISTICS OF THE MAGNETIC FILMS

1. Measurements at 1 KHz

The films used for the r-f memory investigation were first examined with the 1-KHz B-H loop-tracer at the Lincoln Laboratory, M. I. T. The parameters measured were skew angle, α , quartile and 90% dispersion angles, α_q and α_{90} ,⁸ wall coercive field, H_C , hard-axis field, H_K , and wall nucleation field, H_D . Film thickness was derived from the saturation magnetic flux. Generally speaking, skew was within $\pm 1^\circ$, α_q varied between 0.5° and 5° , α_{90} varied between 1° and 10° , H_C and H_D has values in the range 1.5 oe to 2.5 oe, and H_K had values in the range 2 oe to 3.5 oe. Film thicknesses were between 200 \AA and 1200 \AA .

Films of low dispersion, α_q , α_{90} , were also obtained from Lincoln Laboratory, M. I. T.* A summary of the properties of the films which were evaporated in our own laboratory is given in Appendix B.

2. Evaporation of Thin Magnetic Films

The evaporation of films of nickel-iron alloy near the zero magnetostrictive composition of 81 percent Ni, 19 percent Fe, by weight, was made in our laboratory from an electrically-heated, 7 mm. diameter, tungsten helical filament. The source material used was 10-mil alloy wire supplied by Hamilton Watch Co., Precision Metals Division. The composition of the wire was 83 percent Ni, 17 percent Fe, by weight. The choice of using an evaporant of lower iron content is due both to the tendency of the tungsten filament to form an alloy with the nickel and to the higher vapor pressure of iron.⁹ The films were deposited in the presence of a 45-oersted uniform magnetic field onto the heated substrate, placed 24 cm. above the source. The magnetic field induced the direction of the easy axis of magnetization. A

*Grateful acknowledgement is made to T. S. Crowther and M. Naiman, M. I. T. Lincoln Laboratory, for these films.

substrate temperature of 350°C . was maintained by a quartz radiation heater for one hour before evaporation; it was lowered to room temperature during a minimum of two hours following evaporation, throughout which time the 45 oe field was applied. This slow rate of cooling prevented fracture of the films through stress. It was noted that a filament temperature of 1500°C ., measured by an optical pyrometer during evaporation, produced a deposition rate of 50 \AA per second. During evaporation the vacuum system pressure was 10^{-5} torr. All films evaporated from tungsten filaments were observed to have very good adhesion.

Since sequential evaporations from several sources were possible during one pumpdown of our vacuum system, a few multilayer films of NiFe-Cu-NiFe and NiFe-Al-NiFe were evaporated. E. Feldkeller¹⁰ has reported that a significant improvement of thin-film properties is attained by using multilayer film structures having a non-ferrous metal intermediate layer of copper, aluminum, gold, chromium and tin. Interactions between two magnetic layers separated by both ferrous and non-ferrous films have been described in many papers.¹¹⁻¹⁴ Recently, Feldkeller¹⁵ has reviewed the different kinds of interaction. Stein¹⁶ has shown that wall creeping in a pulse field along the hard axis and a d-c field along the easy axis has been observed in multilayer films as well as in single films. However, in contrast to the small fields along the easy axis necessary for wall motion, the field amplitude along the hard axis necessary to cause wall creeping is relatively high in multilayer films.

Our multilayer structures incorporated a layer of either copper or aluminum, of maximum thickness 50 \AA , sandwiched between two 250 \AA NiFe layers. The substrate temperatures used during the NiFe evaporations were 350°C . and 200°C . The higher substrate temperature resulted in films of very large dispersion, presumably due to considerable diffusion taking place from the imbedded layer. The films at 200°C . had improved qualities over those at 350°C . but had either extremely square B-H loops with considerable dispersion ($\alpha_q = 5^{\circ}$, $\alpha_{90} = 10^{\circ}$) for the case of copper, or had very low dispersion ($\alpha_q = 1^{\circ}$, $\alpha_{90} = 2^{\circ}$) with skewed B-H loops, for the case of aluminum. Although these films were, therefore, not tried as memory elements it is

considered that our initial evaporations were sufficiently encouraging to warrant further research with multilayer films.

3. Bitter Pattern Observations

A microscope was specially mounted for Bitter pattern domain observations on a magnetic film still in place within the memory. The main purpose of these observations was to compare the domain patterns produced on continuous sheet, photo-etched and mask-evaporated films. It was observed that even in a "saturation" magnetization condition, there were numerous edge domains running along the edges of etched films. The films were etched in either 20-mil or 40-mil wide strips lying in the direction of the easy axis. Mask-evaporated strips of the same width, on the other hand, did not show these domains, presumably because of those strips having tapered edges.

The procedure of removing the strip transmission lines to observe the domain structure was, however, somewhat tedious, although it was considered essential to leave the magnetic film in place within the memory when observing the domain structure, so that stray field effects would not occur.

C. OBSERVATIONS OF FILM BEHAVIOR IN THE NDRO MODE

During our program of investigating the experimental behavior of films in the NDRO mode, several r-f drive-line configurations were used. In the following discussion of quantitative results, it is to be understood that these refer to one configuration only -- that of a single-strip transmission line and ground plane -- the configuration which gave the least drive-line to sense-line coupling noise. A comparison of the various drive-line schemes is given later.

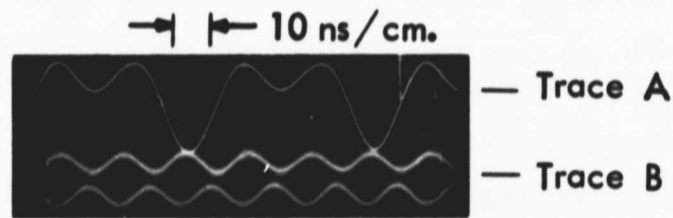
Figure 11c shows the transmission line configuration found to have a minimum of drive to sense-line coupling noise. With the line separations shown, assuming that there is a uniform current distribution over each strip-line cross section, the applied fields in the magnetic film are 8 oersteds/ampere and 10 oersteds/ampere for the 20-MHz and 40-MHz signals, respectively. However, as discussed in Appendix E, those values can vary widely depending on the assumptions of current distribution in the lines. For this reason the results are stated in terms of drive currents rather than applied fields.

Where a single value for r-f drive current amplitude is stated in the following sections of this report, it means that the amplitudes of the 20-MHz and 40-MHz signals were equal.

Unless otherwise stated, all strip-line widths were 20 mils.

1. Film Output Voltage at 60 MHz for Small R-F Signal Drive

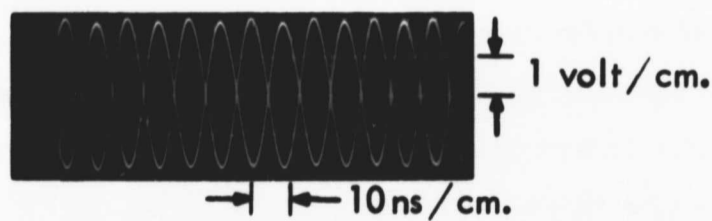
The sense amplifier had a voltage gain of 1700 at 60 MHz, with 40 db voltage rejection at 20 MHz and 40 MHz. The gain was linear up to an output voltage of 6 volts peak-to-peak. Figure 8 shows a typical variation of sense amplifier output voltage film with r-f drive current amplitude. There is excellent agreement with the theoretical variation shown in Fig. 3, assuming an average applied field of 9 oersted/ampere; the value of H_K for the particular film was 2.8 oersteds. Figure 9 shows the variation of sense amplifier output for films of several thicknesses. Oscillographs taken from a Tektronix 585A oscilloscope are shown in Fig. 10a and b. From Fig. 10a it is seen that discernible "0" and "1"



Trace A: Combined drive signal, 20 mA/cm. Vertical

Trace B: Sense amplifier output for both states of magnetization. 0.1 volts/cm. Vertical

(a) Nondestructive readout from 500-Å film with 30 mA, peak-to-peak, 20-MHz and 40-MHz readout drive signals.
Film No. 327



(b) Sense amplifier output from 1000-Å film with 150 mA, peak-to-peak, 20-MHz and 40-MHz readout drive signals.
Film No. 332

Fig. 10 Nondestructive Readout Signals

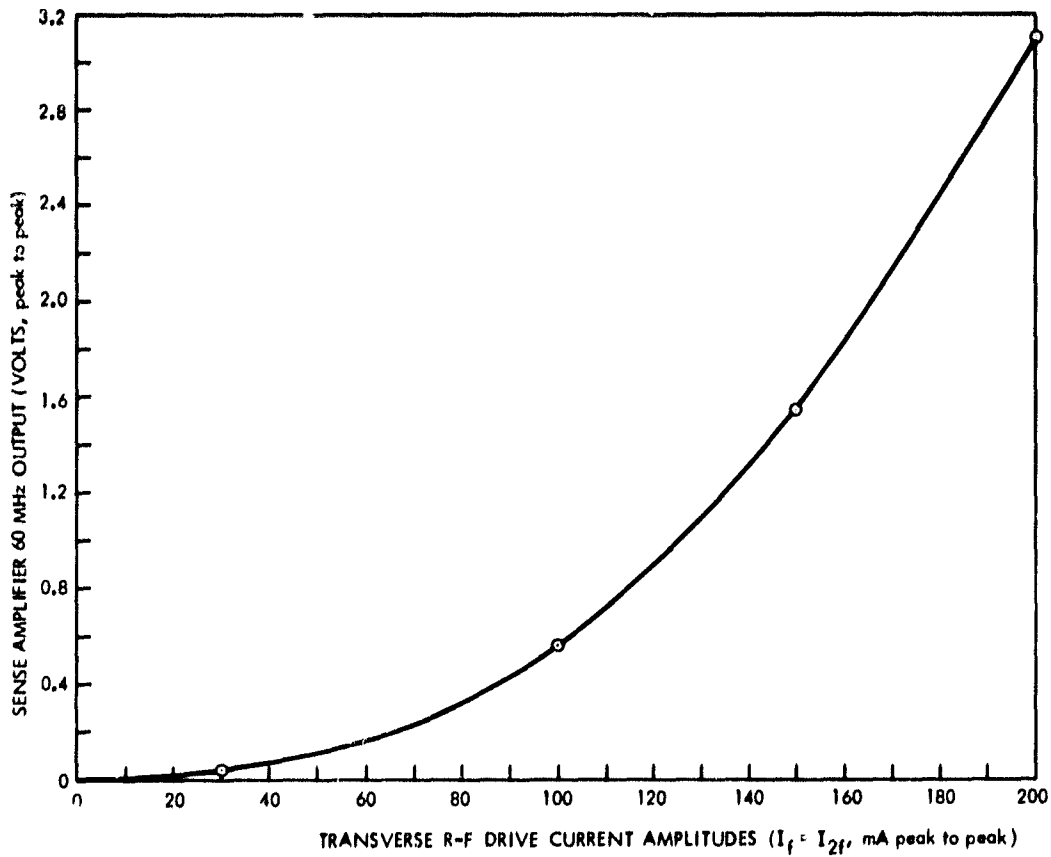


Fig. 8 Variation of Sense Amplifier Output Voltage with Transverse r-f Drive Current Amplitudes in the NDRO Mode. (Film No. 327, Thickness 510 Å. Amplifier gain 1700 at 60 MHz. Line configuration Fig. 11(c), line width 20 mil)

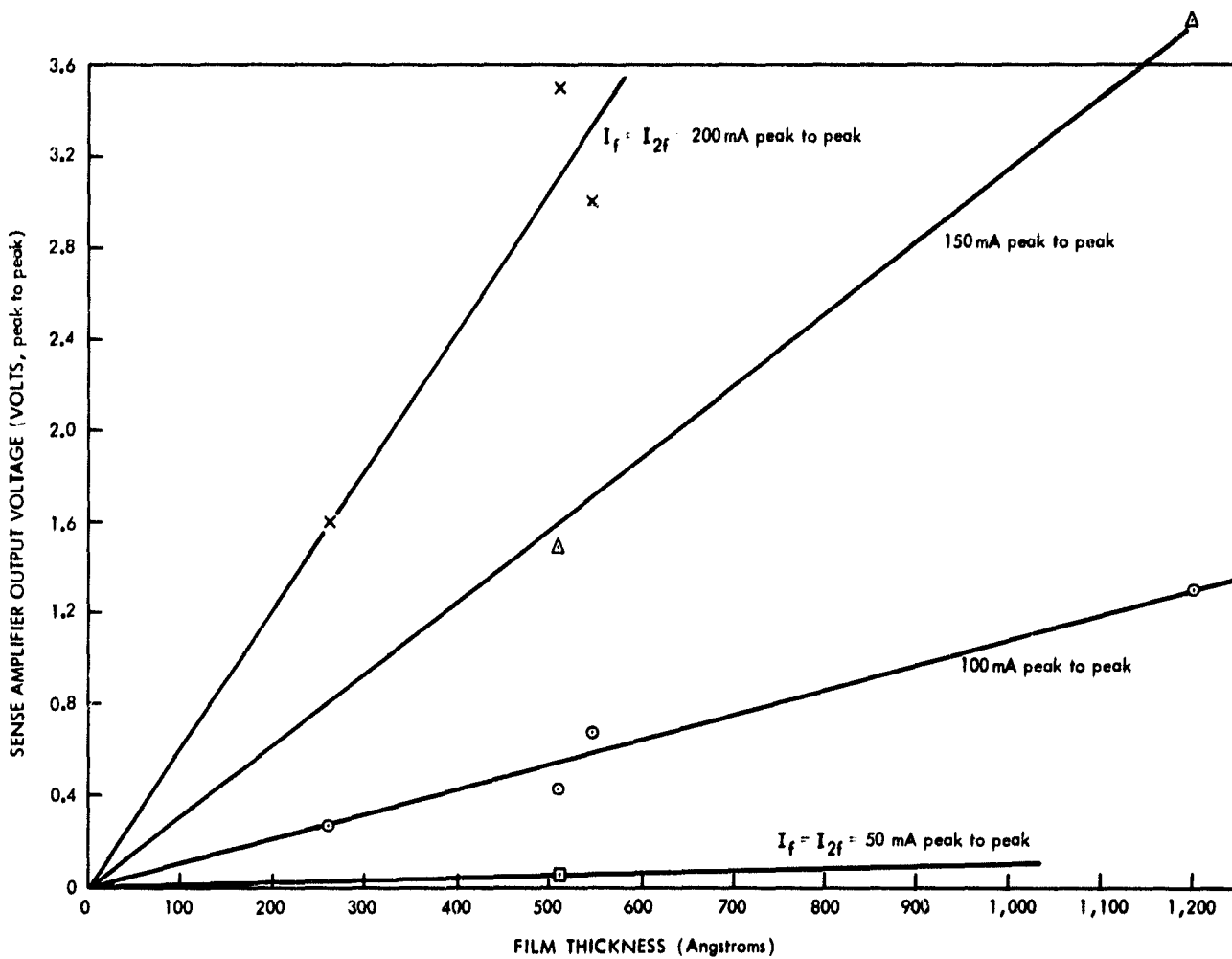


Fig. 9 Variation of Sense Amplifier Output Voltage with Film Thickness for Various NDRO Drive Current Amplitudes. (Line Configuration Fig. 11(c), line width 20 mil)

outputs are feasible with drive currents as low as 30 mA peak-to-peak. The value of 0.04 volt output corresponds to approximately 20 microvolts film output at 60 MHz. By decreasing the line width and separation from the ground plane, the drive currents could have been reduced even further. Figure 10b shows the two outputs for a thicker film and larger drive currents. The drive-line widths were 20 mils. Before each measurement was taken it was verified that the magnetization was stable in both positions and was not disturbed by the readout signal.

2. Disturb Values of Radio-Frequency Drive Currents

For nearly all the films tested, for which H_K had values in the range 2.5 oersteds to 4 oersteds, the 20-MHz and 60-MHz drive currents could be applied up to 200 mA, peak-to-peak, without any disturbance of the sense of magnetization. Most films had a disturb threshold between 300 mA and 400 mA. It was observed that the value for this threshold depended on the field direction corresponding to the peak value of the current amplitude. Thus, again referring to Fig. 6, we see that the current amplitude in one direction is $I_{20} + I_{40}$, that is, $2I_{20}$, whereas in the other direction it is $(9/8)I_{20}$. One might expect disturbance to occur when the field amplitude in either hard-axis direction approached H_K , or in fact entered the region of creep switching (Fig. 2b). This was indeed observed, but it was also observed that the disturbance did not take place equally along both hard directions. Again, several films switched completely to saturation in a preferred easy-axis direction under the influence of the r-f disturb current. Usually this behavior was preceded by a gradual switching, lasting several seconds, to the demagnetized state. This preferential switching was also observed during the pulse writing experiments which are described in Chapter V.

3. The Influence of a d-c Bias Field Along the Easy Axis

The variation of the 60-MHz output signal, increasing with a longitudinal bias field in the direction opposing the magnetization, and decreasing with a bias field in the same direction, was observed. This variation agrees with the predicted variation shown in Fig. 4. The value used for the r-f drive currents was 100 mA peak-to-peak. With

this value it was found possible to omit the horizontal cancellation of the earth's magnetic field and still obtain nondestructive readout. The two 60-MHz output amplitudes (with and without this cancellation) were, of course, different.

An important feature of the r-f readout method described in this report is that the method makes it possible to obtain the inner boundary of the creep region, H_{irr} . This can be found by using a series of increasing amplitudes for the r-f drive currents; for each amplitude the d-c applied field, H_{L0} , is increased until the magnetization is disturbed. This method has the advantage of giving a simultaneous readout of the state of magnetization.

An anomalous effect due to the application of a d-c bias field was noted for several films. When the magnetization was driven to saturation by the application of a longitudinal field from a permanent magnet (approx. 50-100 oersteds at the position of the magnetic film), and the magnet removed, asymmetric output amplitudes in the 60-MHz sense signals were produced when the magnetization was then switched with much smaller d-c fields. In fact, when this condition arose, it was often found that the magnetization would switch spontaneously to one state, although the readout r-f drive signals were well below their disturb threshold. It was further observed that the film could be demagnetized, that is, have no-sense amplifier output, only by applying H_{L0} equal to several times the earth's horizontal component. From this demagnetized state the film could be switched to either magnetized state by a very small change in H_{L0} . In these magnetized states the sense output amplitudes were then equal. The original state of magnetization was obtained only by reversing the magnetization several times with fields of several oersteds. Thus, an effective unidirectional anisotropy was induced by the strong field. This could be the result of regions of locally higher H_K within the film which were normally, that is under the influence of small fields, demagnetized. Under high applied fields these regions became saturated and then contributed to the readout signal.

4. Phase Effects of the NDRO Drive Currents

It was verified that the amplitude of the 60-MHz sense output signal was independent of the relative phase of the 20-MHz and 40-MHz drive signals. An apparent change in the output voltage with phase was traced to a change in the 20-MHz drive-signal amplitude when the phase was altered.

5. Effect of Film Parameters

The NDRO mode was shown to be completely successful for a wide variety of film parameters. Provided the drive amplitudes did not reach the r-f disturb threshold, described above in (3), there was no observable difference in the outputs from the two states of magnetization for films ranging in (α_q, α_{90}) from $(0.4^\circ, 1.0^\circ)$ to $(2.5^\circ, 5.0^\circ)$. As might be expected wall coercive force, H_C , did not have any noticeable effect. The hard-axis anisotropy field, H_K , affected the value for the sense output amplitude, and the disturb threshold, H_{irr} , only to the extent that the disturb threshold is related to the value for H_K .

6. Comparison of Continuous Sheet, Photo-etched, and Mask-evaporated Films

The magnetic films tested were either in the form of a continuous sheet or a line in the direction of the easy axis. The width of the line was 20-mil or 40-mil, produced by photo-etching or by evaporation through a machined mask. Most of the films were continuous sheet films. The main difference between the behavior of the different forms of films in the readout mode, apart from different r-f disturb thresholds, was in the noise coupling between drive and sense lines. In general, the r-f disturb threshold, H_{irr} , for a line film produced by etching from a continuous sheet film was higher than that for the same film in its continuous sheet form, although etching reduced the values for H_C and H_K .

For continuous sheet films the drive to sense line noise was much lower than for line films. As discussed in the following section, (7), this noise was mainly due to a 60-MHz component added to the 20-MHz and 40-MHz drive signals. It could, therefore, have been reduced by improving the waveshape of the drive signals.

From Bitter patterns it was observed that mask evaporated films had fewer domains under "saturation" than had the etched line films.

7. Comparison of Transmission Line Configurations

Three r-f drive-line configurations were investigated. These are shown in Fig. 11a, b, and c. Configurations (a) and (c) are

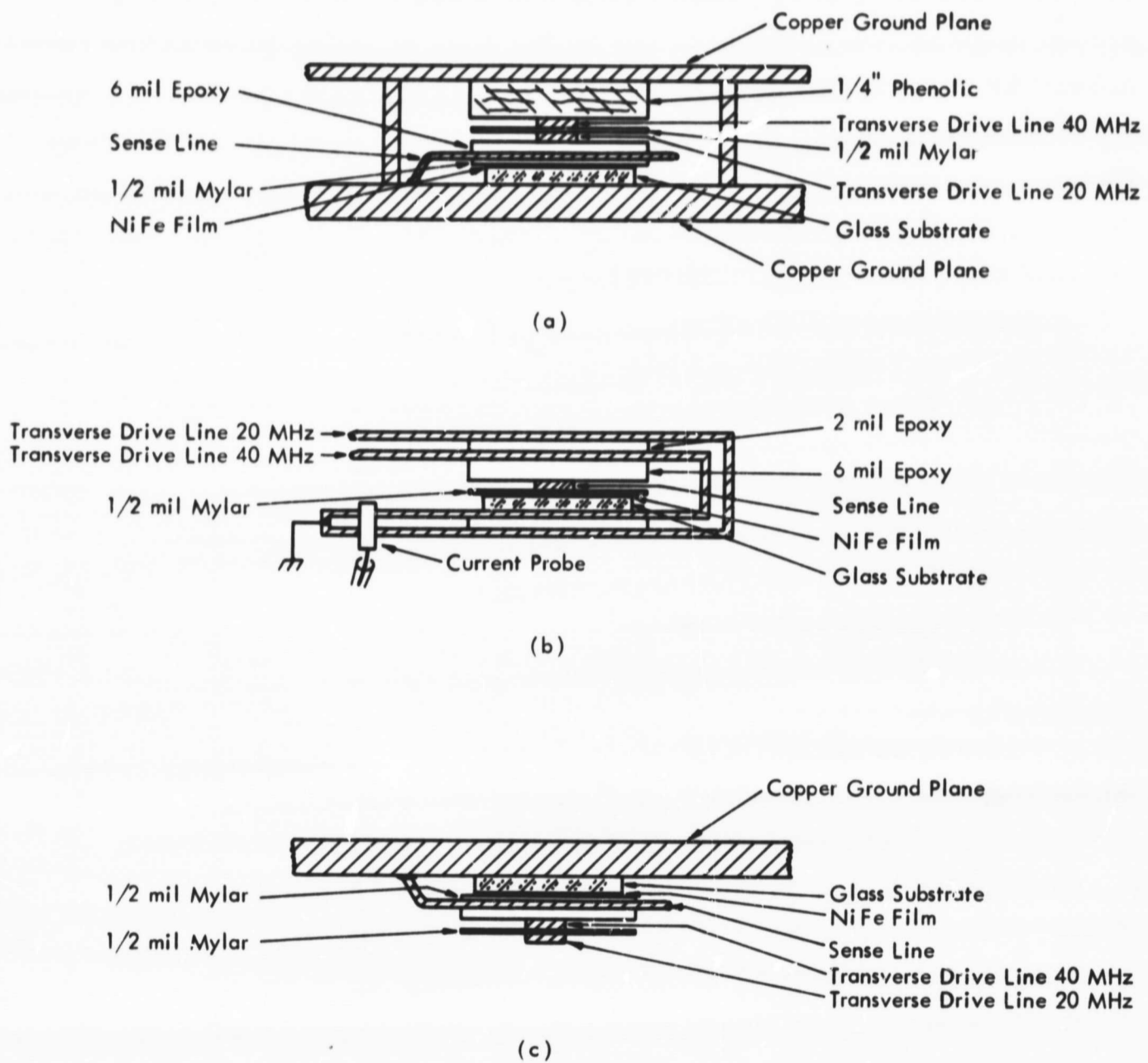


Fig. 11 Transmission Line Configurations

basically the same, consisting of a single stripline over a ground plane. However, in (a) the ground plane was connected by four shorting bars to another, more remote, ground plane on the opposite side of the stripline. This second ground plane was the one used for the main sense

amplifier circuitry. The reason for assembling the memory in this way was to provide easy access for interchanging the magnetic film. However, considerable 60-MHz noise appeared at the sense amplifier output in this configuration by clamping the film magnetization with the field of a permanent magnet (200-400 oersteds); this was shown to be system-produced noise. The noise was found to originate from stray ground plane currents. These currents were apparently the result of connecting the two ground planes by the four shorting bars at the corners. The line width used in configuration (a) was 40 mils.

In configuration (b) the ground plane was eliminated and folded lines were used. The line width was also reduced from 40 mils to 20 mils. The 60-MHz noise in this configuration, however, was much greater than for configuration (a).

Configuration (c), in which a single ground plane and 20-mil-wide drive and sense lines were used, proved by far the most successful configuration tried. With (c) we were able to obtain equal and opposite phase 60-MHz outputs of amplitude 4.0 volts peak-to-peak, having a noise output of only 70 mv peak-to-peak. As the noise was observed to originate entirely in the 40-MHz signal, any improvement in the wave-shape of this signal would have virtually eliminated the noise. It is also to be noted that since the noise appeared as the result of applying one of the drive frequencies, it represented the half-select signal output.

The use of radio-frequencies in the 20-MHz to 40-MHz range was, therefore, shown to be a very successful technique for nondestructive readout. This was demonstrated for films having a wide variety of creep thresholds and a wide range of dispersion angles.

CHAPTER IV

THEORETICAL BASIS FOR COINCIDENT PULSE AND COINCIDENT RADIO-FREQUENCY WRITE SCHEMES

Thin-film memory write schemes may be classified as word-organized, or coincident-current. As discussed in Chapter I, Introduction, a coincident-current method provides a large saving in selection circuitry over a word-organized one.

In compatible operation in a thin-film memory the same transverse fields are used in the write mode as in the read mode. This is desirable for reasons of economy and is not very difficult to achieve in a word-organized, destructive readout memory, since there is then no upper bound for the transverse field. In practice this field is very large, being two or three times H_K . In a word-organized NDRO memory, however, the readout transverse pulse field, H_T , must be smaller than the switching threshold field. In this NDRO memory the question is then whether writing can be accomplished by a longitudinal field, H_L , in coincidence with a transverse field H_T , when H_L is such that it alone does not disturb the magnetization. For most practical films, H_L must be fairly small to avoid causing wall motion, and H_T must be smaller than the disturb threshold field. Their combination then may not be enough to cause full rotational switching, in which case different transverse fields must be used in the read and write modes. However, the increased circuitry to control the amplitude of the transverse field can be compensated by the fact that no rewriting operation is necessary in an NDRO memory.

In noncompatible operation, that is when a different H_T is used in the read and write modes, there is still no upper bound for H_T in the write mode of a word-organized memory, except that the fringing field at neighboring bits must be tolerably small. In a coincident-current memory, however, H_T is bounded by the condition that the combined $H_T/2$ and H_L must not disturb the sense of the magnetization in half-selected cells. Also, the repeated application of $H_T/2$ and H_L must not disturb half-selected cells, which depends on the value for the creep threshold, H_{irr} . Moreover, H_T and H_L together

must fully switch the magnetization. Keeping $H_T/2$ and H_L low to avoid creep switching means that coherent rotational switching may then be impossible by a single application of H_T and H_L .

A memory scheme based on creep switching is possible,¹⁷ which utilizes the phenomenon that magnetization reversal can take place under the simultaneous application of a train of transverse field pulses and a longitudinal d-c field. A recent review of domain wall-creeping has been given by S. Middelhoek and D. Wild.¹⁸ However, no satisfactory creep memory is known to exist,

A scheme based on radio frequencies for both transverse and longitudinal fields is possible. It was believed that the tendency for creep switching would be effectively reduced, based on the intuitive observation that the magnetization would move symmetrically during alternate half cycles.

A description of the pulse and r-f write schemes is given in the following sections.

A. COINCIDENT PULSE WRITING

Coincident pulse writing is well known and is described here only briefly. In Fig. 12a the total fields for half-selected cells (A) and fully-selected fields (B) are indicated relative to the regions of creep and incoherent switching. It is obvious that these regions are predominant in determining whether coincident operation is possible.

An important parameter in considering the feasibility of coincident pulse-writing is the selection ratio. This is defined as the ratio of total word current for fully-selected cells to the maximum total word current for other cells. In Appendix D it is shown that the selection ratio in an ordinary selection scheme is two. For a scheme in which bias currents are applied to the drive lines to inhibit disturbance of the magnetization the maximum possible selection ratio is three. However, as is shown in Appendix D, a selection ratio of three is possible only at the cost of considerable power. For coincident pulse-writing, therefore, it is essential to obtain films which either have suitable material properties or have some particular geometry to permit a selection ratio of two.

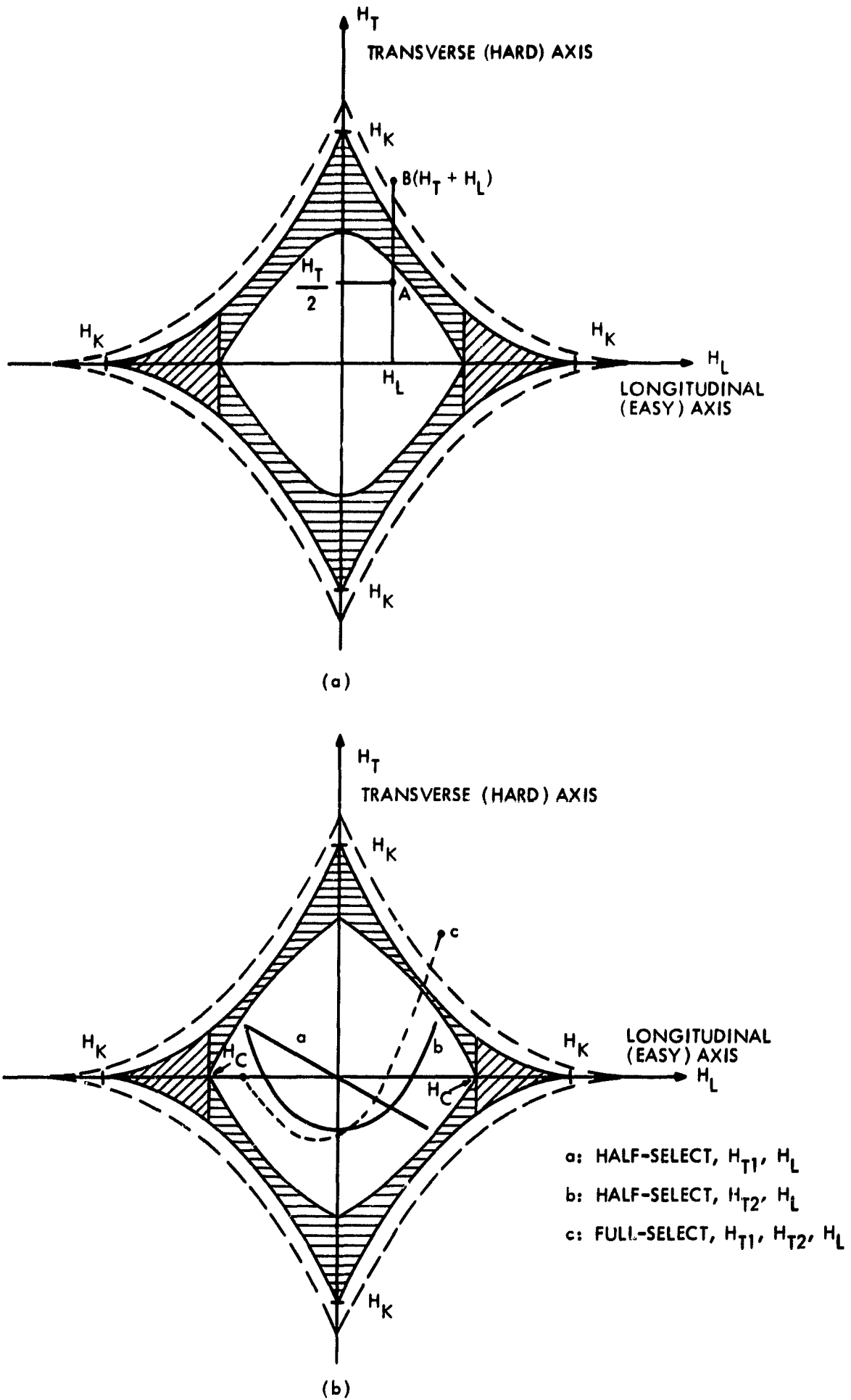


Fig. 12 Schemes for (a) Coincident Pulse Writing and (b) Coincident Frequency Writing

B. COINCIDENT RADIO-FREQUENCY WRITING

A method of coincident-frequency writing compatible with the NDRO r-f mode utilizes the same transverse-axis drive signals that are used for transverse-axis excitation during nondestructive readout. An additional sinusoidal excitation along the easy axis, with either 0° or 180° phase relationship, determines the state of magnetization that is written into the selected cell. Whereas phase relationship is irrelevant in the readout mode, phase coherence between all components of excitation is required in the write mode. A r-f scheme of writing was proposed as it was believed to offer less creep disturbance than conventional pulse-writing schemes.

It is theoretically possible to write using either "even" or "odd" modes. Even-mode writing is one in which the frequency, ω_2 , of the second transverse excitation is an even multiple of the first frequency, ω_1 . The frequency of the longitudinal excitation is also ω_1 . In odd-mode writing the transverse excitations have frequencies ω_1 , ω_2 which have an odd integer ratio. The longitudinal excitation, which again contains the information to be stored in its phase, 0° or 180° , has a frequency that is twice that of the lower-frequency, transverse-axis excitation, ω_1 .

1. Even-Mode Writing

The excitations for even-mode writing are

$$\begin{aligned} h_{T1} &= H_{T1} \cos\omega_1 t \\ h_{T2} &= H_{T2} \cos\omega_2 t, \quad \omega_2 = m\omega_1, \quad m \text{ an even integer} \\ h_L &= \pm H_L \cos\omega_L t, \quad \omega_L = \omega_1 \end{aligned}$$

The simplest case, $m=2$, is compatible with the readout mode investigated, using the same transverse fields for writing and readout. Figure 12b shows the loci of the applied fields for the cases of half-selected cells (a and b) and for a fully-selected cell (c). In cases (a) and (b) the loci remain within the critical switching curve, or, more exactly, within the disturb-threshold curve. In case (c), both transverse excitations are applied simultaneously with the longitudinal excitation, and the locus of the resultant applied field traverses a region

of rotational switching. Depending on the phase of ω_L , this region corresponds to one or the other easy-axis direction.

2. Odd-Mode Writing

The excitations for odd-mode writing are

$$h_{T1} = H_{T1} \cos\omega_1 t$$

$$h_{T2} = H_{T2} \cos\omega_2 t; \quad \omega_2 = n\omega_1, \quad n \text{ an odd integer}$$

$$h_L = \pm H_L \cos\omega_L t; \quad \omega_L = 2\omega_1$$

The simplest case, $n=1$, might give adequate writing; however, it does not provide compatible coincident readout selection, the lowest compatible case having $n=3$. As in even-mode writing, the sense of the magnetization following a write excitation is determined by the phase of the longitudinal (digit) excitation, 0° or 180° .

3. Comparison of Even- and Odd-Mode Writing

A comparison of even- and odd-mode writing is best made by considering which will allow compatible operation with the readout mode. In the readout mode we can define a frequency margin, ω_m , as the frequency difference between $\omega_1 + \omega_2$, the desired sum frequency, and either the nearest sideband, ($2\omega_1$, $2\omega_2$, or $\omega_2 - \omega_1$), or the nearest system noise frequency, (ω_1 or ω_2), produced by nonorthogonality of the drive-sense lines. It will be shown that the system-produced noise frequency, ω_2 , constitutes the major limitation to the frequency margin. If the sidebands alone are considered, the frequency margin is given by

$$\omega_m = \pm(\omega_2 - \omega_1)$$

from the $2\omega_1$ and $2\omega_2$ sidebands, and by

$$\omega_m = 2\omega_1$$

from the $(\omega_2 - \omega_1)$ sideband. ω_m , therefore, rises linearly from zero, when $\omega_2/\omega_1 = 1$, to a maximum value of $2\omega_1$, when $\omega_2/\omega_1 > 3$.

If both sidebands and system produced noise are considered, the frequency margin is again given by

$$\omega_m = \pm (\omega_2 - \omega_1) \text{ and } 2\omega_1$$

from the sidebands, and by

$$\omega_m = \omega_1 \text{ and } \omega_2$$

from the system-produced noise frequencies. ω_m , in this case, rises linearly from zero, when $\omega_2/\omega_1 = 1$, to a maximum value of ω_1 , when $\omega_2/\omega_1 \geq 2$. In view of the likely presence of system-produced noise, the optimum ω_m has a value equal to ω_1 , when $\omega_2 = 2\omega_1$. This is the even-mode system, which permits the use of compatible readout and writing modes.

CHAPTER V

EXPERIMENTAL OBSERVATIONS OF COINCIDENT PULSE AND COINCIDENT RADIO-FREQUENCY WRITE SCHEMES

As explained in Chapter IV there are several fundamental difficulties to obtaining coincident-write operation. The main difficulty is that the critical switching curve defining the boundary between regions of rotational switching and nonswitching may be quite widely separated by regions of domain wall motion and incoherent switching. In addition, even for ideal films having an exact critical curve, there is also a variety of reasons why films do not switch according to the simple single-domain model. The main factors are nonuniformity of drive fields applied through strip lines, demagnetizing fields, film shape and edge effects, eddy currents in the drive lines and films, and capacitive coupling between the lines. A detailed discussion of some of these factors is given in Appendix E.

In view of these difficulties an experimental investigation was undertaken to examine the following aspects of both coincident-pulse and coincident r-f write schemes:

1. Using the nondestructive readout r-f method, to obtain the amount of flux switched by applying single current pulses simultaneously to both longitudinal and transverse drive lines.
2. Using the nondestructive readout r-f method, to obtain the amount of flux switched by applying a train of current pulses ($> 10^5$ pulses) simultaneously to both longitudinal and transverse drive lines.
3. To attempt to obtain conditions of coincident r-f write and compare the results with the behavior of the films under pulse writing.
4. To investigate whether a hybrid system of r-f transverse fields and pulsed longitudinal fields would give coincident operation.

A. COINCIDENT PULSE-WRITE EXPERIMENTS

Pulse-writing measurements were made using the same test apparatus used for the NDRO investigation, shown in Fig. 7. Both drive line configurations (a) and (c) of Fig. 11 were used with no significant

differences in the results other than the quantitative differences produced by configuration (a) having 40-mil-wide drive lines and configuration (c) having 20-mil-wide drive lines. The transverse current pulses, I_T , providing fields along the hard axis, were obtained from an EH 132A pulse generator. The same transverse drive lines were used for writing as for readout. The longitudinal current pulses, I_L , providing fields along the easy axis were obtained from an EH 138 pulse generator. The sense line was also used for applying the longitudinal (easy-axis) write field. It was found possible to synchronize the pulse generators by driving the EH 132A external drive input from the EH 138 trigger output. It was important, however, to terminate the 50-ohm cable connecting the pulse generators at the EH 132A input. This was done to eliminate multiple pulse triggering of the EH 132A. Synchronization of the current pulses, I_T and I_L , was adjusted by displaying the outputs of Tektronix CT-2 current probes on a 585A oscilloscope. Attention was paid to having the probe 50-ohm output cables of the same length and to terminating them at the oscilloscope.

The pulse durations were generally 80 nanoseconds for I_T and 270 nanoseconds for I_L . These pulses were unipolar and rectangular, with negligible overshoot at the beginning and end of each pulse.

Before each series of pulse-write experiments was carried out for any particular magnetic film, the nondestructive readout drive current amplitude was increased to find the disturb level. During the subsequent pulse-write measurements the readout drive current was kept at an amplitude well below this disturb level. For most films tested the value of 200 mA peak-to-peak for both the 20-MHz and 40-MHz signals was well below this level. The procedure for pulse writing was first to drive the film to saturation with the aid of a permanent magnet field. This field ranged from 50-100 oersted. The synchronized transverse and longitudinal single pulses were then applied. Next, the readout drive currents were applied and the amount of flux switched was measured as a percentage of the saturation value. Measurements were made for both $\pm I_L$ and $\pm I_T$ pulses, so that all four quadrants of the switching curve were investigated. The measurements were repeated for a train of pulses (greater than 10^5 pulses) and the results plotted for both single-pulse writing and many-pulse writings. As shown in Figs. 13, 14, 15, and 16, our observations all indicated

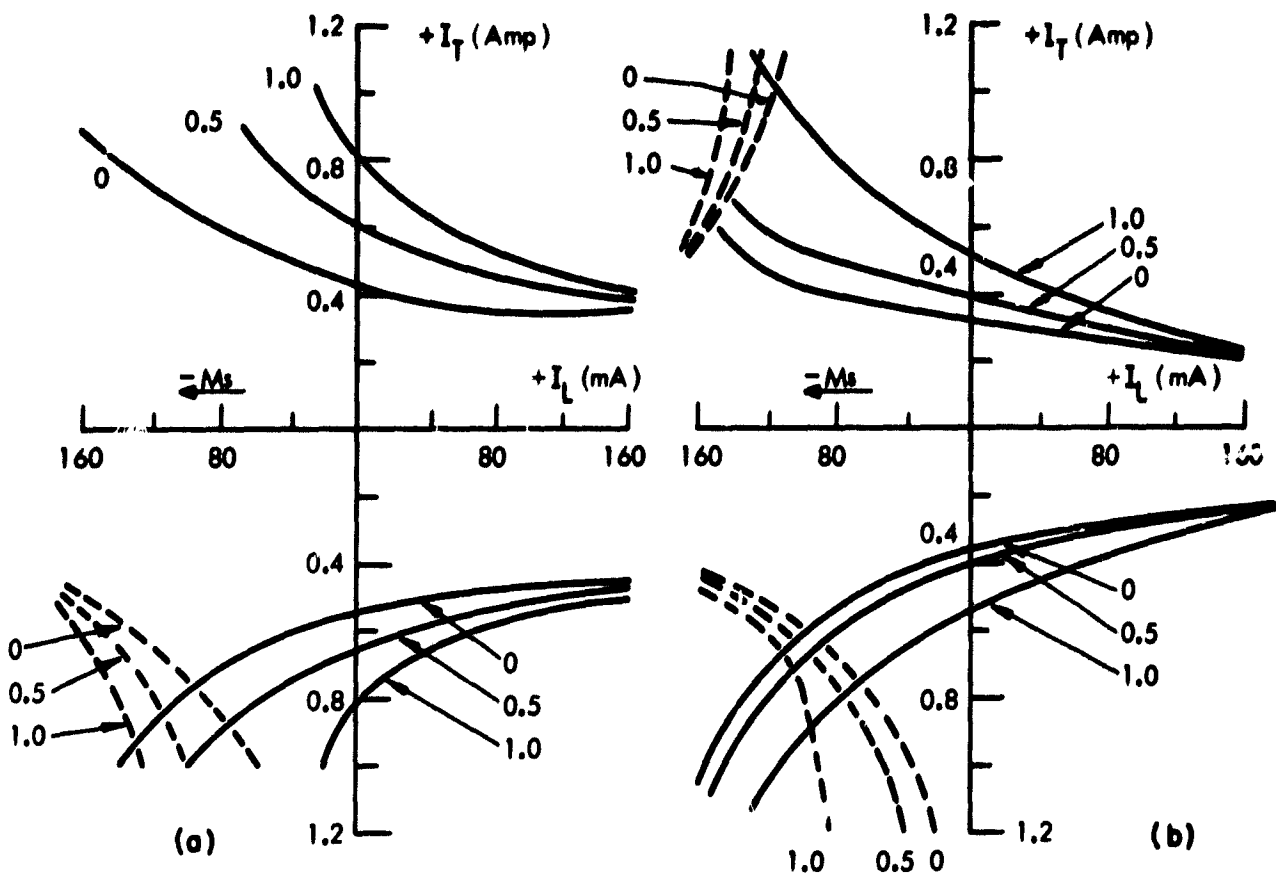


Fig. 13 Coincident Pulse Writing. Film No. 327
(a) Single Pulse Pair, (b) Greater than 10⁵ pulses

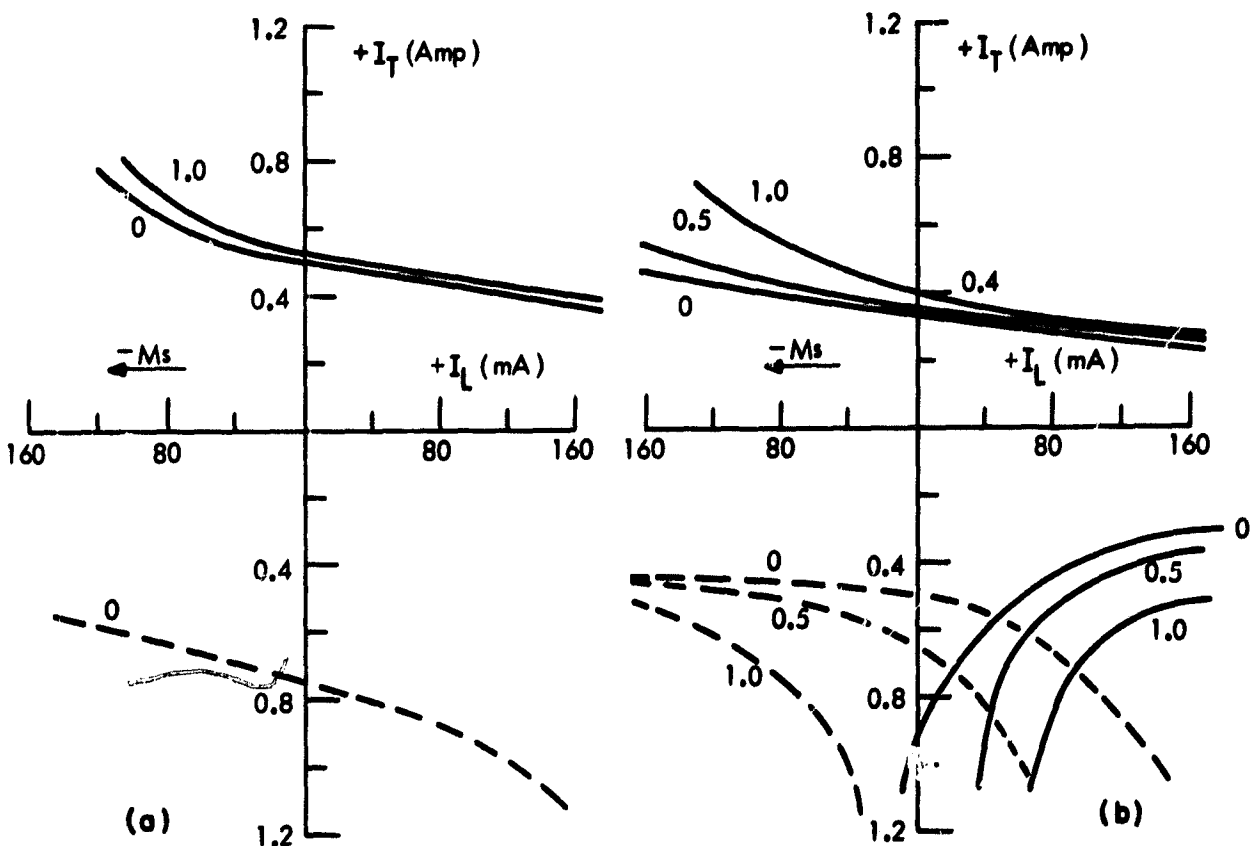


Fig. 14 Coincident Pulse Writing. Film No. 332
(a) Single Pulse Pair, (b) Greater than 10⁵ pulses

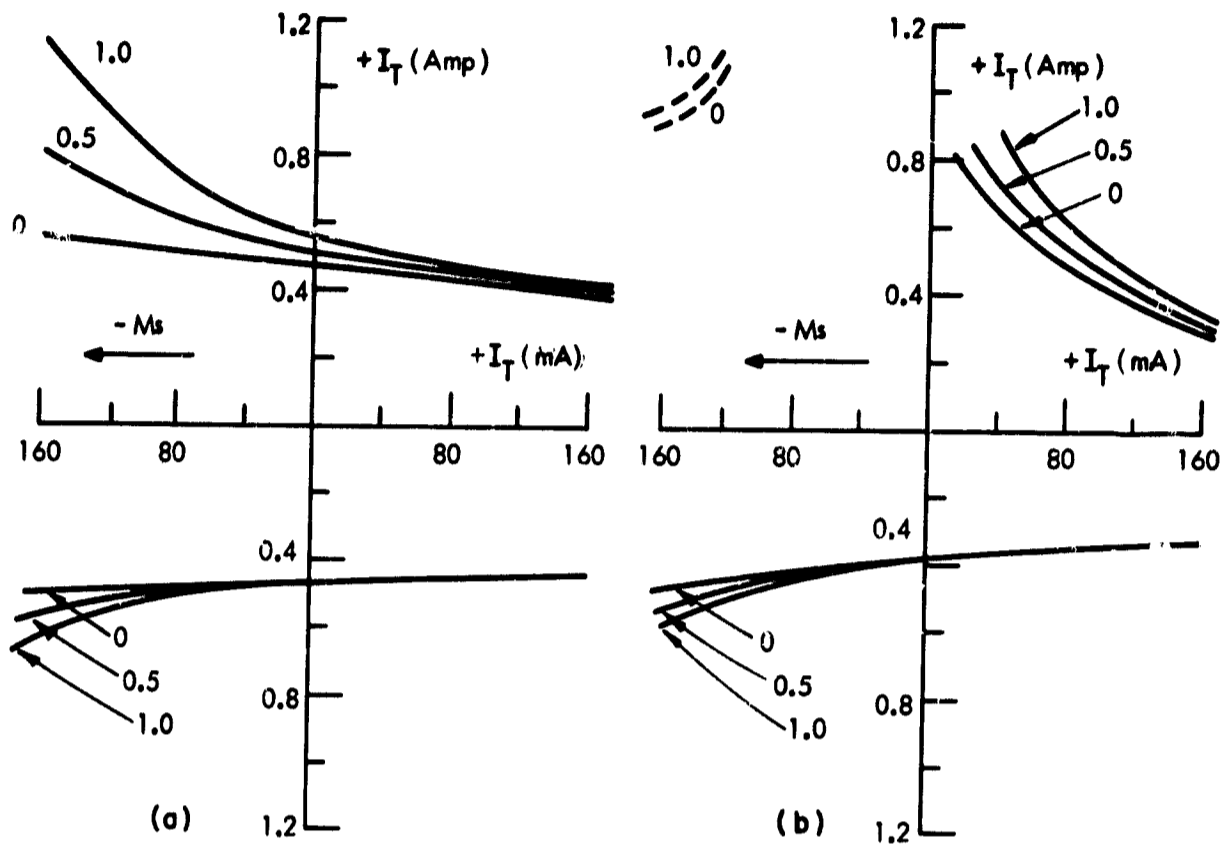


Fig. 15 Coincident Pulse Writing. Film No. 210P6B
 (a) Single Pulse Pair. (b) Greater than 10^5 pulses

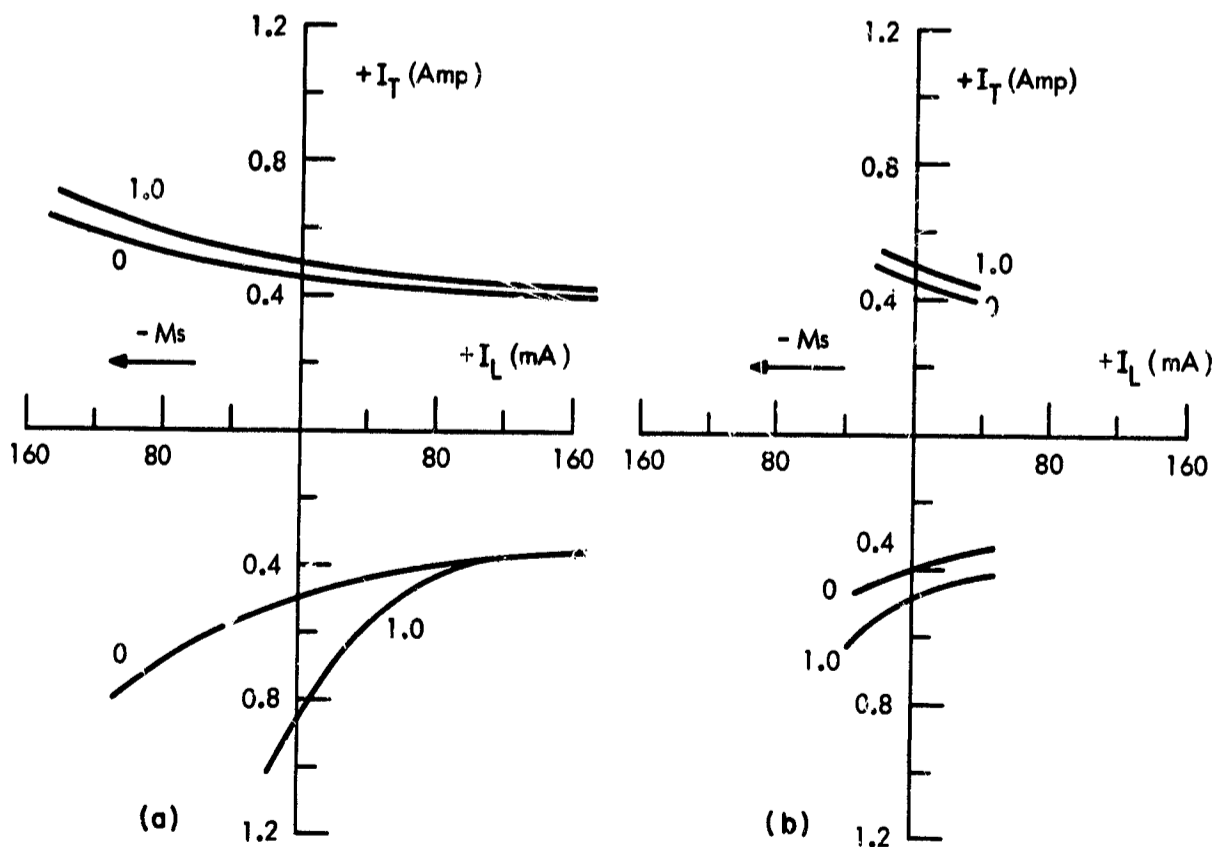


Fig. 16 Coincident Pulse Writing. Film No. 337
 (a) Single Pulse Pair, (b) Greater than 10^5 pulses

regions of anomalous switching. The curves labelled 0, 0.5, and 1.0 indicate the respective boundaries where some disturbance to the magnetization takes place, where the magnetization is switched to half of its possible saturation value, and finally to complete saturation. The continuous curves represent the results of applying $\pm I_T$, together with $+ I_L$ steering pulses to a film originally saturated in the $- M_s$ direction. The $- M_s$ direction is the direction which should result from $- I_L$ steering pulses. The dotted curves correspond to an initial state of saturation in the $+ M_s$ direction. The drive-line widths used for the data of Figs. 13-16, were 40 mils with the relatively large line-to-film spacing of at least 40 mils, resulting from the thick substrates. From these line widths and line-to-film spacings the applied fields at the position of the films, assuming a uniform current density distribution in the lines, are $H_T = 5.5$ oe/amp and $H_L = 6.8$ oe/amp. These values are calculated for a position in the film directly underlying the center line of the drive conductor. The calculations were based on Appendix E, Eq. E.4. As is observed from Figs. 13-16, the switching regions investigated were close to the transverse axis, that is, for small longitudinal fields.

The observed curves are seen to be anomalous in that switching occurred when a combination of hard-axis and easy-axis fields was applied which should have left the direction of magnetization unchanged. The effect of any uncompensated earth's horizontal component field can be ruled out since this field was measured as 0.18 oersted. This was compensated to within ± 0.01 oersted. The presence of overall easy-axis skew can also be eliminated since this was within $\pm 1^\circ$; even a large deviation from this value over localized regions of the film would not account for the differences in switching behavior resulting from different initial magnetization settings, $\pm M_s$. The influence of the readout drive signals can also be ruled out, since these signals were always each less than 200 mA, peak-to-peak, which gave a resultant peak amplitude of less than 200 mA. Moreover, the readout amplitude was checked as being nondestructive for each film examined. This was done not only for the case of complete saturation of the film in both senses, but also for intermediate states obtained by breaking the film into domains by a permanent magnet. It is believed

that the observed effects may have been due either (1) to a history-dependent effect in which the result of applying an easy-axis pulsed field depends on the amplitude of the previous easy-axis field, or (2) to the demagnetizing fields of the surrounding continuous sheet film. In case (1), the easy-axis field applied before each pulse writing was that of a permanent magnet, approximately 50-100 oersteds. It is believed that effective changes in the anisotropy took place similar to those described in Chapter III, Section C3. The regions of higher coercive force may well have been in the form of a layer.^{12, 19} In case (2), it is not believed that the demagnetizing field would result in such a definite reversal of the magnetization.

It was evident from those results that continuous films, having parameters similar to those of the films investigated, would be completely unsuitable for coincident pulse write. The effects of pulse write were attempted for films etched to form 40-mil or 20-mil wide strips with their length along the easy axis. The most promising result was obtained with a 250 Å, 20-mil wide etched strip film. However, it was reduced to a nearly demagnetized state when subjected to a series of write pulses of alternately opposite, $\pm I_L$, easy-axis polarity.

In view of these results, it was decided to compare a coincident r-f write scheme applied to films of similar characteristics to those tested in the pulse-write scheme.

B. COINCIDENT RADIO-FREQUENCY WRITING

For the investigation of coincident r-f writing the experimental arrangement of Fig. 7 was again used, having 20-mil wide drive lines, as in configuration (c) of Fig. 11. The fields, again according to the assumption of uniform current density distribution in the drive lines (as analyzed in Appendix E), are $H_T = 9$ oersteds/ampere, $H_L = 12.5$ oersteds/ampere. The compatible even mode write scheme with $\omega_2/\omega_1 = 2$ was chosen, with $\omega_1 = 20$ MHz. Gating was not attempted other than by a manually operated switch. The r-f write investigated, therefore, corresponded to the case of many-cycle writing.

Coincident operation was observed for several continuous sheet films but only provided a small d-c bias, H_{DC} , equal to 0.20 oersted to 0.25 oersted was applied along the easy axis. The direction of this bias corresponded to that in which the film was being switched. It

might be considered that this was simply a special case of creep-writing in which creep occurred under the simultaneous application of a sinusoidal transverse field and a d-c longitudinal field. However, it was verified that the presence of the r-f longitudinal field was also necessary for switching to occur. Again, the phase of this field relative to the transverse field was important.

The currents I_L and I_T were plotted against one another for the conditions of writing and nonwriting. The writing condition was that when true coincidence held, that is, the application of the longitudinal 20-MHz signal, in combination with either the 20-MHz or the 40-MHz transverse signal, did not disturb the magnetization, whereas the combination of all three signals produced full switching of the magnetization. The nonwriting condition was one in which the phase of the longitudinal 20-MHz signal was altered slightly, so that writing no longer occurred. The results are shown in Fig. 17. This plot was derived from dual-trace oscilloscope waveforms of the total transverse drive current and longitudinal drive current. It shows the resultant locus of the drive current. Figure 18 shows a similar plot in which the resultant current locus is given for another set of phase conditions under which coincident writing occurred. In this figure, however, the separate loci for the longitudinal 20-MHz current in combination with either component of the transverse current are shown.

From the results it is clear that the simple theoretical conditions for writing under the application of r-f drive currents did not hold.

C. DISCUSSION OF COINCIDENT RADIO-FREQUENCY WRITING

Several points are immediately obvious from the results of the particular r-f writing technique used. First of all, coincident frequency writing was only achieved with the simultaneous application of a small longitudinal d-c bias field in the direction of writing. The application of a small transverse d-c bias field was not investigated during writing. Secondly, the phase of the longitudinal drive current was important in determining whether or not writing occurred, although it did not have the behavior predicted. Finally, the amplitude of the longitudinal drive current required for writing was very much larger than the transverse drive current amplitudes.

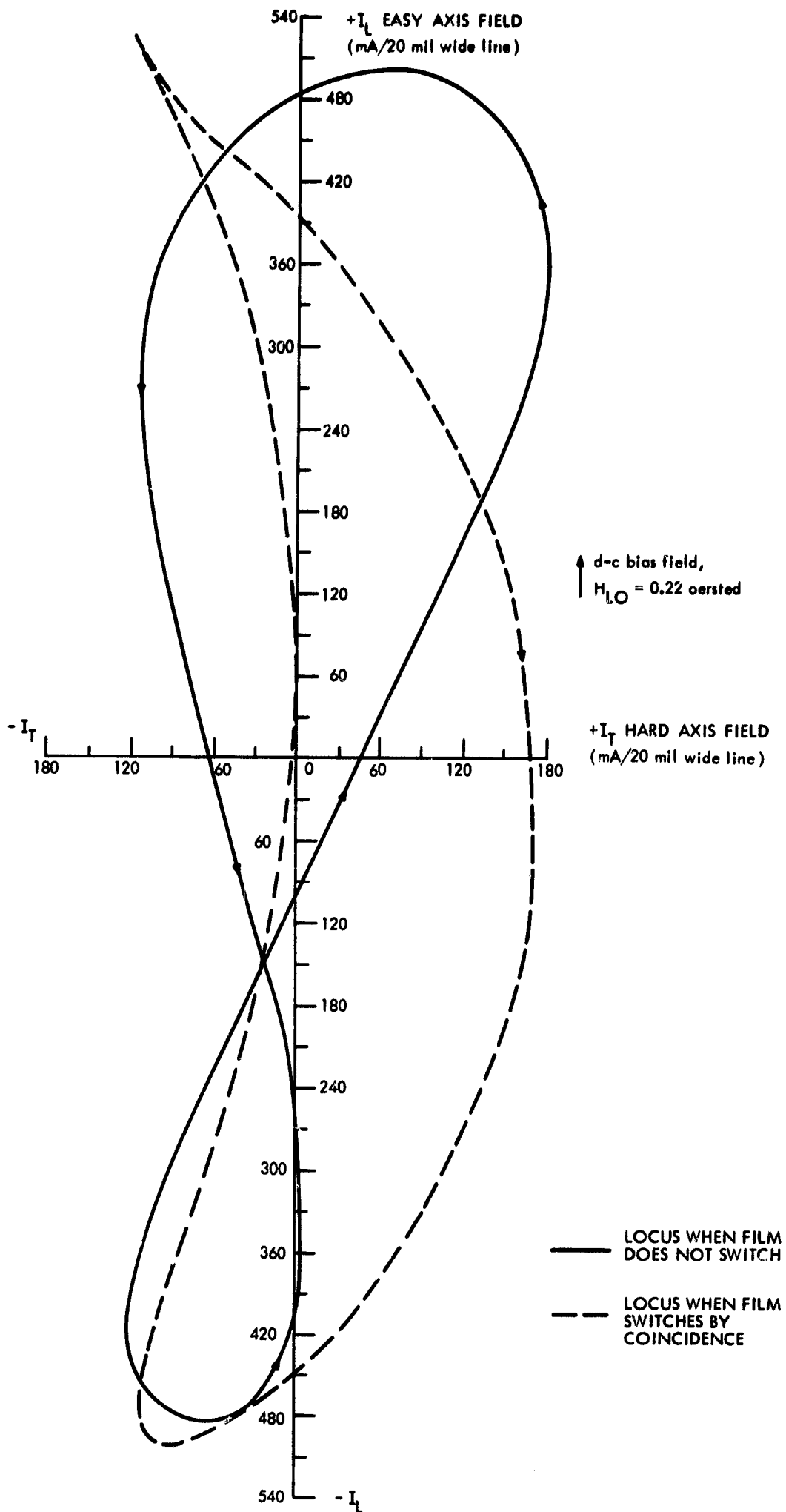


Fig. 17 Switching Field Loci for Coincident Frequency Writing and Non-writing. Film No. 328. Hard Axis Drive Frequencies 20 MHz + 40 MHz. Easy Axis Drive Frequency 20 MHz

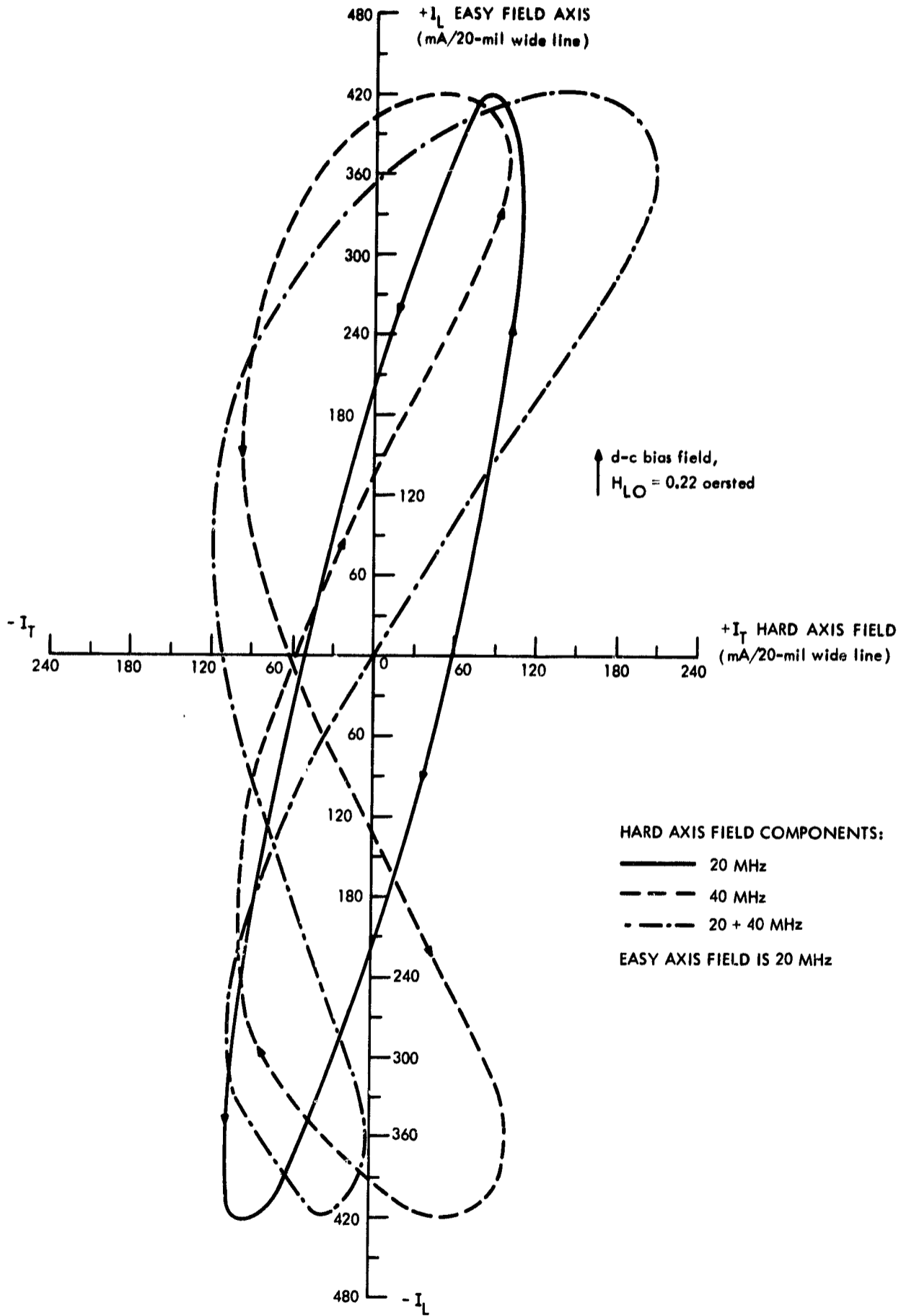


Fig. 18 Switching Field Loci for Coincident Frequency Writing. Film No. 328. 20 MHz and 40 MHz Components of Hard Axis Drive Field Shown Separately. Easy Axis Drive Frequency 20 MHz

It is possible that the observed writing occurred by means of a domain wall creep mechanism since the presence of a d-c longitudinal bias field was necessary. However, it is significant that the presence of this d-c bias alone, together with the transverse r-f drive currents was insufficient for writing to occur. The discrepancy in the phase conditions is not understood. It is noted, however, that writing occurred when the resultant applied field locus (assuming the simple strip-line model) took the form of a cusp in the direction of writing. It is suggested that a more exhaustive examination of the change in this locus throughout all phase conditions, when writing was observed, would have shown closer agreement with the theoretical model. The large amplitude required in the longitudinal drive current would have been greatly reduced by the use of much thinner substrates, and it is possible that the conditions for writing would then have been closer to the theoretical model.

CHAPTER VI

CONCLUSIONS

A. COINCIDENT RADIO-FREQUENCY NDRO

The use of a r-f technique to obtain coincident nondestructive readout was successfully demonstrated. Using drive currents of 20 MHz and 40 MHz during readout, it was observed that the values of these currents could be as low as 30 mA peak-to-peak and still give discernible output signals of opposite phase. The drive lines used for this measurement were 20-mil wide strip lines, separated from a single ground-plane by the 40 mil thickness of the glass substrate. The drive currents could obviously be reduced further by using narrower drive lines and thinner substrates, especially metal substrates used as the ground plane.

Only manual keying of the readout signals was investigated, but throughout the investigation this was never observed to disturb the direction of magnetization. The duration of the signals required for readout is, therefore, unknown, but it is considered that the method would be as successful for still higher frequencies.

B. COINCIDENT RADIO-FREQUENCY WRITING

Coincident r-f writing was only obtained with difficulty, having the additional requirements of a d-c biasing field and critical phase adjustments. However, it is significant that a coincident mode of writing was achieved for films which proved to be completely unsuitable for coincident pulse writing. As in the readout investigation, manual keying of the drive signals was used, so that the minimum time for writing is unknown.

Since the coincident r-f write mode examined still appeared to be limited by domain wall creep and incoherent rotational switching, the investigation was not pursued further.

C. SUGGESTIONS FOR FUTURE INVESTIGATIONS

The investigation described in this report was aimed at demonstrating the feasibility of coincident r-f techniques as applied to a small scale thin-magnetic film memory. Relatively unsophisticated methods were used, in that the investigation did not, for example, involve using finely-etched, narrow-width, drive lines, a large array of memory cells, or metal substrates; nor did it involve closed film structures, plated wires, etc. It is suggested, therefore, that any future investigation using these techniques should include the following:

1. A comparison of metal substrates with thinner glass substrates than were used for this investigation.
2. Much narrower drive-line widths.
3. The influence of keying the r-f drive signals, and any subsequent noise introduced when a larger memory array is examined.
4. The use of films other than simple single-layer NiFe films. These might include multilayer films having a sandwich layer of SiO_2 or ferrite-coated films.
5. The use of closed flux films such as plated wires, etc.
6. The use of different mask-evaporated cell geometries.

APPENDIX A

FLOW CHART OF THE COMPUTER PROGRAM TO FIND θ FROM A GIVEN H_L AND H_T

As described in Chapter II, Section B, the computer program was in three successively run parts. The first part obtained the total transverse and longitudinal drive fields, H_T and H_L . The second part determined θ from the minimum energy condition, Eq. 2:

$$H_K \sin\theta \cos\theta + H_L \sin\theta - H_T \cos\theta = 0$$

that is

$$f(\theta) = 0$$

and from the stability condition

$$f'(\theta) \geq 0$$

The third part determined the output voltage from the value of θ satisfying the above two conditions. A flow chart of the second part is given in Fig. 19.

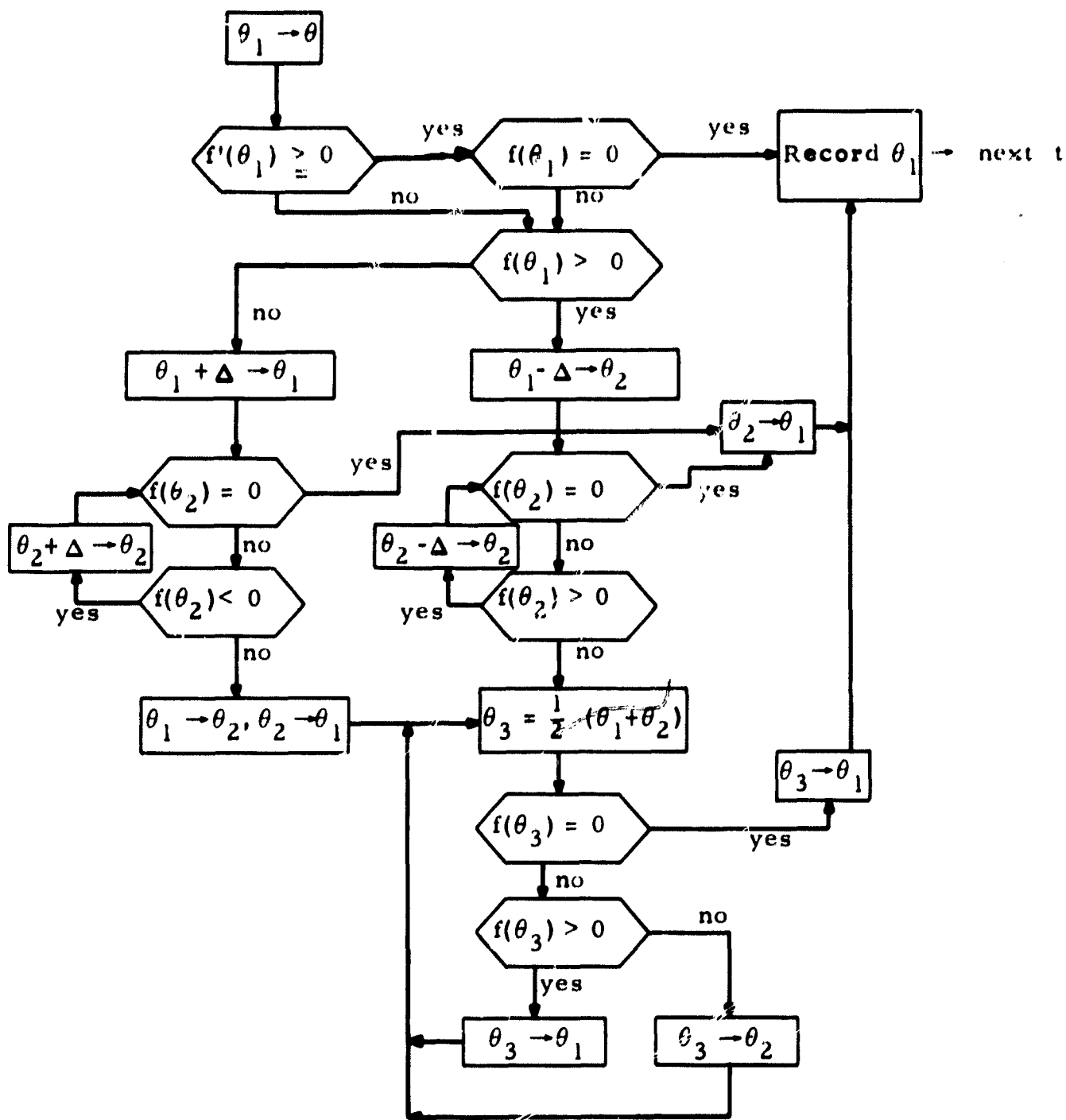


Fig. 19 Flow Chart of the Computer Program to find θ from a given H_L and H_T

APPENDIX B

SUMMARY OF PARAMETERS OF FILMS EXAMINED

Table B. 1 provides a summary of the parameters of the films examined, including data on the evaporation procedure for films fabricated in our laboratory, and the memory test performance of those films and films obtained from Lincoln Laboratory. The films fabricated in our laboratory were evaporated in an oil-diffusion pumped system having a residual pressure in the low-to-mid 10^{-6} torr range.

The following notes refer to Table B. 1.

1. Film numbers in 300 series were evaporated in our laboratory. Other numbers refer to those obtained from M. I. T. Lincoln Laboratory.
2. The wire lengths quoted are those of the pre-alloyed 83:17, NiFe wire, 0.010" diameter, used as evaporant. The evaporations were normally made from a single tungsten helical filament 5.0 cm long and 0.8 cm diameter. "Double source" refers to the use of two filaments. "Continuous" refers to a continuous sheet film. "Mask line width" refers to a film mask-evaporated in a line pattern along the easy axis.
3. Film thickness measured from value for saturation flux density obtained with loop tracer.
4. Drive-line configurations A, B, C refer to Fig. 11a, b, c respectively.
5. This is the NDRO transverse disturb drive current, I_f or I_{2f} , with zero easy-axis field.
6. "Induced asymmetrical NDRO outputs" refers to the asymmetry induced by the 50-100 oersted field used to set the magnetization in a saturated condition.
7. "Pulse writing asymmetry" refers to the anomalous pulse writing behavior which was observed.
8. Domain structure of film within the memory observed by Bitter technique. After "saturation" pulse write, considerable domain structure existed:

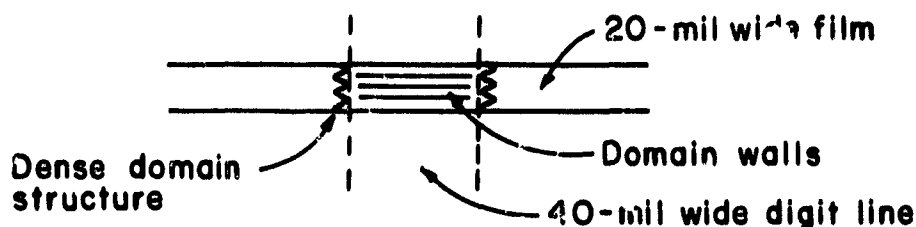


TABLE B. 1

Film No. (1)	Substrate Evaporation Temp. (°C)	Notes on Evaporation Procedure (2) (source-substrate distance 25 cm)	1000 Hz Hysteresis Loop Tracer Measurements					Anisotropy Field, H_K (oersteds)	
			Film (3) Thickness (angstroms)	Skew Angle α (degrees)	Quartile Dispersion Angle, α (degrees)	90% Dispersion Angle, α_{90} (degrees)	Wall Nucleation Field, H_D (oersteds)		Coercive Force, H_C (oersteds)
300	300°C	33 cm wire continuous	145 Å	-1°	7°	11°	1.1	1.3	2.8
301	300°C	133 cm wire continuous							
304	300°C	133 cm wire mask line width 40 mils	≈500 Å	-	0.15°	0.6°	1.6	2.25	3.2
309	300°C	33 cm wire mask line width 40 mils	≈200 Å	-	-	-	1.2	1.5	2.2
311	300°C	33 cm wire mask line width 40 mils	≈200 Å	-	-	-	1.4	1.5	2.6
312	300°C	33 cm wire mask line width 40 mils	≈200 Å	-	-	-	1.5	1.8	3.0
318	350°C	133 cm wire slow cooling with field applied	655 Å	0°	0.9°	4.2°	1.5	2.1	2.3
320	350°C	220 cm wire double source continuous	1000 Å	+1°	0.9°	3.7°	2.2	3.6	2.6
321	350°C	330 cm wire triple source	1200 Å						
323	350°C	33 cm wire slow evaporation continuous film	155 Å	0°	4°	8°	1.5	1.5	3.5
324	350°C	33 cm wire continuous	60 Å	0°	2°	3.6°	1.0	1.0	4.4
325	350°C	85 cm wire continuous	200 Å	0°	4.7°	8.2°	1.45	2.2	3.4
327	350°C	85 cm wire continuous	510 Å	+1°	0.4°	1.0°	1.25	2.1	2.8
328	350°C	140 cm wire continuous	620 Å	0°	1.4°	3.0°	1.7	2.2	2.8

Memory Performance			
Film No.	Drive-Line (4) Configuration A, B, or C and Line Width	NDRO Disturb (5) Drive Current Amplitude (mA peak-to-peak)	Comments on Film Behavior under NDRO Writing, or by Domain Wall Observation.
300			
301	A, 40 mils	> 400 mA	Successful NDRO. Induced asymmetrical NDRO outputs observed (6).
304			Used for domain observations only. No walls observed along mask-formed edges.
309			
311			
312			
318			
320	A, 40 mils		Successful NDRO. Pulse-writing asymmetry (7) first observed for this film.
321			
323	C, 20 mils	400 mA	Successful NDRO.
324			
325	C, 20 mils		Successful NDRO.
327	A, 40 mils	> 300 mA	Successful NDRO. Induced asymmetrical NDRO outputs (6).
	B, 20 mils	> 200 mA	NDRO obtained, but configuration gives large sense output noise.
	C, 20 mils	> 300 mA	Successful NDRO. Readout obtained from completely demagnetized state using 100 mA peak-to-peak drive. Excellent readout for very low drive currents. Pulse-writing asymmetry. (7)
328	C, 20 mils		Successful NDRO. R-F writing shown feasible under certain conditions.

TABLE B. 1 (Contd.)

Film No. (1)	Substrate Evaporation Temp. (°C)	Notes on Evaporation Procedure (2) (source-substrate distance 25 cm)	1000 Hz Hysteresis Loop Tracer Measurements						
			Film Thickness (3) (angstroms)	Skew Angle α (degrees)	Quartile Dispersion Angle, α_q (degrees)	90% Dispersion Angle, α_{90} (degrees)	Wall Nucleation Field, H_D (oersteds)	Coercive Force, H_C (oersteds)	Anisotropy Field, H_A (oersteds)
329	350°C	140 cm wire continuous	545 Å	0°	3.7°	8.9°	1.5	2.3	2.7
330	350°C	170 cm wire double source continuous	890 Å	+2°	2.4°	5.2°	2.0	4.2	2.0
331	350°C	170 cm wire double source continuous	855 Å	+1°	2.7°	5.0°	1.0	5.4	2.4
332	350°C	220 cm wire double source continuous	1000 Å	+1°	2.4°	4.6°	1.7	2.1	2.8
333	350°C	220 cm wire double source continuous	910 Å	+1°	5.9°	10.4°	2.0	2.2	2.7
335	350°C	50 cm wire mask line width 20 mils	270 Å	-0.5°	-	-	1.5	1.5	2.6
336	350°C	60 cm wire mask line width 20 mils	315 Å	-0.5°	-	-	1.4	1.6	3.0
337	350°C	70 cm wire mask line width 20 mils	395 Å	+1°	-	-	1.7	1.7	3.0
340	350°C	85 cm wire 8.9 mg Cu 85 cm wire	815 Å	-0.5°	2.9°	6.6°	2.8	3.5	3.0
341	350°C	85 cm wire 10.9 mg Cu 85 cm wire	710 Å	+1°	9.7°	14.5°	1.25	2.1	3.3
345	200°C	85 cm wire 8.9 mg Cu 85 cm wire	890 Å	0°	5°	10°	2.2	2.5	4.0
346	200°C	85 cm wire 10.9 mg Al 85 cm wire	835 Å	0°	1°	2°	0.7	1.2	3.9

Memory Performance			
Film No.	Drive-Line (4) Configuration A, B, or C and Line Width	NDRO Disturb (5) Drive Current Amplitude (mA peak-to-peak)	Comments on Film Behavior under NDRO, Writing, or by Domain Wall Observation.
329	C, 20 mils		Successful NDRO R-F writing shown feasible under certain conditions.
330			
331	C, 20 mils		
332	A, 40 mils C, 20 mils	400 mA	Successful NDRO
333	A, 40 mils		Successful NDRO Induced asymmetrical NDRO outputs (6).
335			Successful NDRO.
336			Successful NDRO.
337	A, 40 mils	450 mA	Domain structure along one edge only. Possibly due to tapering of one edge of film.
340		}	Successful NDRO obtained. Not tested in write mode.
341			
345			
346			

TABLE B. 1 (Contd.)

Film No. (1)	Substrate Evaporation Temp. (°C)	Notes on Evaporation Procedure (2) (source-substrate distance 25 cm)	1000 Hz Hysteresis Loop Tracer Measurements						
			Film (3) Thickness (angstroms)	Skew Angle α (degrees)	Quartile Dispersion Angle, α (degrees)	90° Dispersion Angle, α_{90} (degrees)	Wall Nucleation Field, H_D (oersteds)	Coercive Force, H_C (oersteds)	Anisotropy Field, H_K (oersteds)
210P6B	—	continuous	750 Å	0°	0.8°	1.6°	1.5	1.8	2.6
210P8B	—	40 mil wide etched strips	820 Å	0°	0.8°	1.6°	1.6	1.8	2.4
345P8A	—	20 mil wide etched strips	375 Å	0°	0.5°	1.2°	1.9	1.8	3.4
348P0A	—	40 mil wide etched strips	460 Å	+2°	0.6°	1.3°	1.7	1.7	3.2
575P8B	—	continuous	1000 Å	-1°	0.65°	1.2°	3.2	3.4	2.8
581P14A	—	continuous	1170 Å	0°	0.9°	1.6°	2.3	2.2	3.3
585P1A	—	continuous	1400 Å	0°	0.65°	1.8°	2.2	2.4	2.9

Memory Performance			
Film No.	Drive-Line ⁽⁴⁾ Configuration A, B, or C and Line Width	NDRO Disturb ⁽⁵⁾ Drive Current Amplitude (mA peak-to-peak)	Comments on Film Behavior under NDRO, Writing, or by Domain Wall Observation.
210P6B	A, 40 mils		Asymmetry of pulse writing. ⁽⁷⁾ The anomalous difference between single pulse and creep writing is believed due to differences between the strengths of the d-c saturation fields used to set the magnetization.
210P8B	A, 40 mils	> 400 mA	Many cross-tie walls observed along etched edges. Strong 40 MHz component in NDRO from film.
210P8A	A, 40 mils	> 400 mA	"Saturation" pulse write domain structure observed. ⁽⁸⁾ Asymmetry of pulse writing. ⁽⁷⁾
345P8A	A, 40 mils		Domain wall (with numerous cross-tie walls) runs parallel to etched edge, when film "saturated".
575P8B	A, 40 mils		Successful NDRO. Used for domain observations.
581P14A	A, 40 mils		Successful NDRO.
585P1A	A, 40 mils		Successful NDRO.

APPENDIX C

MAGNETIC FIELD OF SQUARE HELMHOLTZ COILS

The most accurate method which we found for setting up (x, y) component fields cancelling the horizontal component of the earth's magnetic field was first to arrange all three (x, y, z) component cancelling fields. In this way, when cancellation was complete, a Bell Model 240 Gaussmeter probe at the position later occupied by the magnetic film, could be rotated in any direction with no observable flux. The coil system was then rotated until there was no component of the earth's field along the transverse, y-axis. The vertical, z, cancelling field was then dispensed with, as demagnetizing fields normal to the plane of a magnetic film are much larger than the earth's field.

The most convenient coil arrangement for the vertical, z, cancelling field was a square Helmholtz pair. Although the solution of the optimum separation of the coils and field strength at the center is straightforward, it was not found to be readily available in the literature. It is, therefore, included here. Since this solution was obtained, a computer solution, which includes the off-axis field pattern, has become available.*

The axial component, H_1 , of the field of a single turn square coil of side $2a$ cm., at a point, P, distance y cm. along the axis from the center of the coil is readily obtained from the Biot-Savart Law:

$$\vec{H} = \frac{I}{10} \int \frac{d\vec{s} \times \vec{r}}{r^3} \text{ oersted} \quad (I \text{ in amperes}) \quad (\text{C. 1})$$

From Fig. 20,

$$H_1 = \frac{4I}{10} \int \left(\frac{1}{r^3}\right)(\sin\alpha)(|d\vec{s} \times \vec{r}|) \quad (\text{C. 2})$$

*Firester, A. H., "Design of Square Helmholtz Coil System", Review of Scientific Instruments, Vol. 37, No. 9, 1966, p. 1264.

$$\begin{aligned}
 H_1 &= \frac{4I}{10} \int_{-\pi/4}^{\pi/4} \left[\frac{\cos^3 \phi}{(a^2 + y^2 \cos^2 \phi)^{3/2}} \right] \left[\frac{a}{(a^2 + y^2)^{1/2}} \right] \left[\frac{a(a^2 + y^2)^{1/2}}{\cos^2 \phi} \right] d\phi \\
 &= \frac{4I}{10} \int_{-\pi/4}^{\pi/4} \frac{a^2 \cos \phi d\phi}{(a^2 + y^2 \cos^2 \phi)^{3/2}} \\
 &= \frac{4Ia^2}{5(a^2 + y^2)(2a^2 + y^2)^{1/2}} \tag{C.3}
 \end{aligned}$$

To obtain the optimum separation, $2y$, for a square Helmholtz pair of coils each of N turns, we can find the field at an axial point, P , distance ϵ from the mid-point, C , between the coils, Fig. 21. By expanding binomially we can obtain the axial component, H_P , of the field at P in terms of ϵ , ϵ^2 , etc.

$$H_P = \frac{4NIa^2}{5(a^2 + (y+\epsilon)^2)(2a^2 + (y+\epsilon)^2)^{1/2}} + \frac{4NIa^2}{5(a^2 + (y-\epsilon)^2)(2a^2 + (y-\epsilon)^2)^{1/2}} \tag{C.4}$$

$$\text{Let } C = \frac{4NIa^2}{5(a^2 + y^2)(2a^2 + y^2)^{1/2}}$$

Then

$$\begin{aligned}
 H_P = C \left[4 - \frac{2\epsilon^2}{(a^2 + y^2)} - \frac{\epsilon^2}{(2a^2 + y^2)} + \frac{8y^2\epsilon^2}{(a^2 + y^2)^2} + \frac{3}{4} \frac{4y^2\epsilon^2}{(2a^2 + y^2)^2} \right. \\
 \left. + \frac{4y^2\epsilon^2}{(a^2 + y^2)(2a^2 + y^2)} + \dots \right] \tag{C.5}
 \end{aligned}$$

Setting the coefficient of ϵ^2 to zero reduces to

$$-5a^6 + 11a^4y^2 + 18a^2y^4 + 6y^6 = 0 \tag{C.6}$$

This is of the form

$$Y^3 + pY^2 + qY + r = 0 \tag{C.7}$$

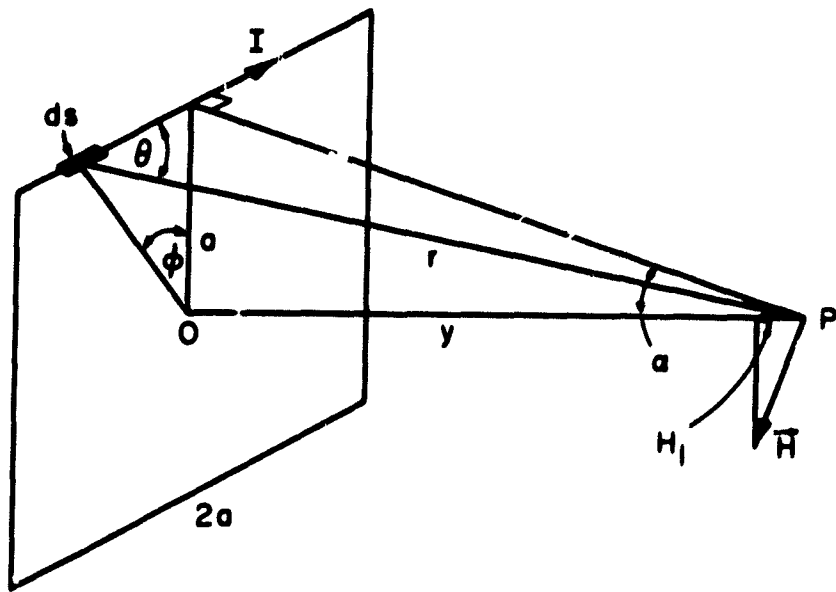


Fig. 20 Field Diagram of a Single Turn Square Coil

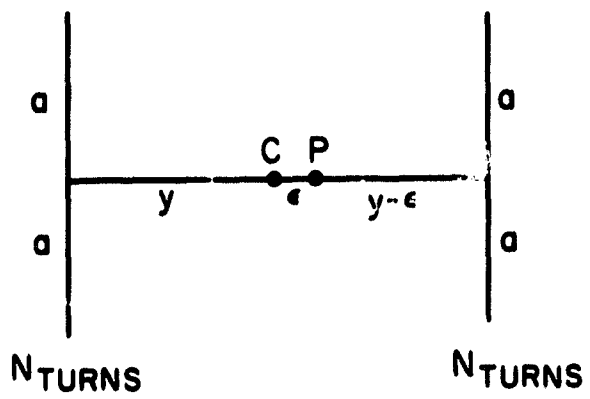


Fig. 21 Distances used in Calculating Square Helmholtz Coil Separation

which reduces to²⁰

$$x^3 + Ax + B = 0 \quad (C. 9)$$

by the transformation

$$y^2 = Y = x - p/3 = x - a^2$$

$$A = \frac{1}{3}(3q - p^2) = -\frac{7}{6}a^4 \quad (C. 9)$$

$$B = \frac{1}{27}(2p^3 - 9pq + 27r) = -\frac{2}{3}a^6$$

The solution is then

$$x = \left[-\frac{B}{2} + \left(\frac{B^2}{4} + \frac{A^3}{27} \right)^{1/2} \right]^{1/3} + \left[-\frac{B}{2} - \left(\frac{B^2}{4} + \frac{A^3}{27} \right)^{1/2} \right]^{1/3} \quad (C. 10)$$

$$= a^2 [0.5620]^{1/3} + a^2 [0.1046]^{1/3}$$

$$= 0.825a^2 + 0.471a^2 = 1.296a^2$$

$$Y = x - a^2 = 0.296a^2$$

$$y = 0.544a \quad (C. 11)$$

The optimum coil separation, S, is, therefore, in terms of the length of a side, 2a,

$$\frac{S}{2a} = 0.544 \quad (C. 12)$$

The field for this separation is

$$H = \frac{8NIa^2}{5(a^2 + 0.544^2 a^2)(2a^2 + 0.544^2 a^2)^{1/2}} \quad (C. 13)$$

$$H = \frac{1.630 NI}{2a} \text{ oersted} \quad \left\{ \begin{array}{l} N \text{ turns} \\ I \text{ amperes} \\ a \text{ cm.} \end{array} \right. \quad (C. 14)$$

APPENDIX D

SELECTION RATIO FOR COINCIDENT-CURRENT WRITING

The operation of writing in a coincident-current memory requires two word currents, A and B, for word selection in addition to the digit current carrying the information to be written (either ONE or ZERO). For nonselected word lines, word currents a and b may be supplied to inhibit any destruction in half-selected cells. A bias field d which may be constant or may be switched on only during the write mode may also be applied to all the cells to inhibit destruction in nonselected cells.

Then the cells in a fully-selected word receive the total word current of $A + B + d$, while half-selected cells receive either $A + b + d$ or $a + B + d$ and nonselected cells receive $a + b + d$, as in Fig. 22.

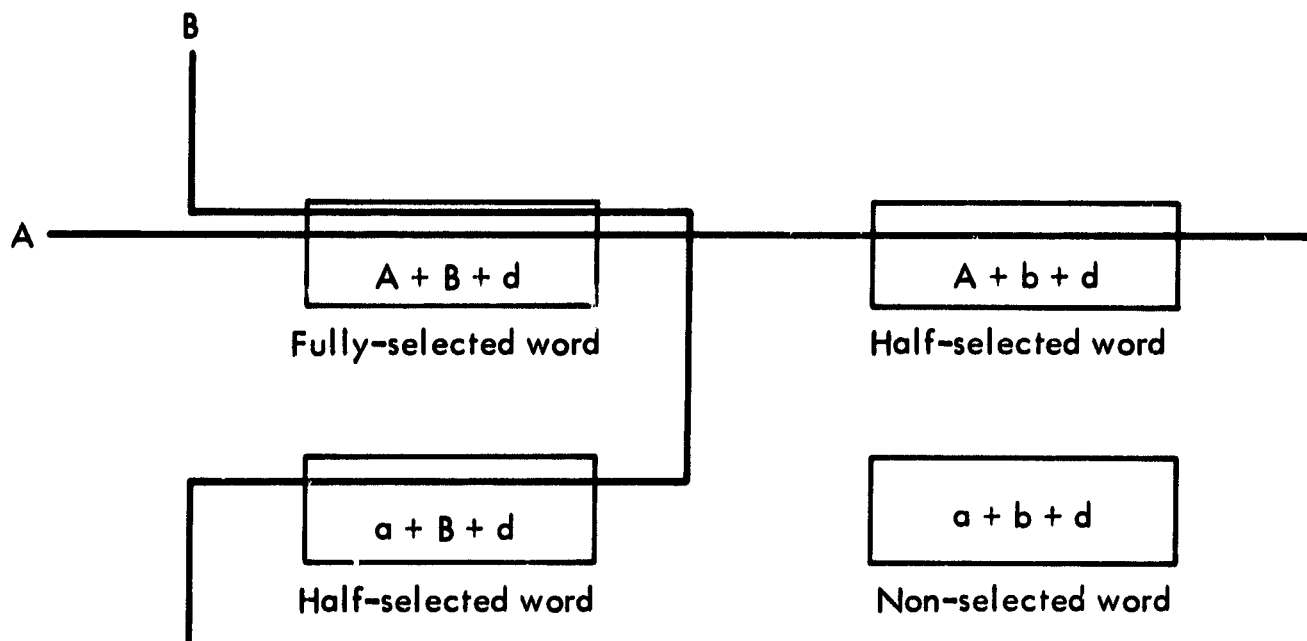


Fig. 22 Word Drive Currents used in Obtaining the Selection Ratio

It is interesting to consider how much total current can be applied to fully-selected cells when the total currents for half-selected and non-selected cells are limited to within a certain range (say, 1 in arbitrary units), determined by the digit current. Let us define a Selection Ratio as the ratio of the total word current for fully-selected cells to the maximum total word current for other cells. While this ratio is 2 in an ordinary selection scheme, using $A = B = 1$ and $a = b = d = 0$, it

will be shown that the maximum possible ratio is 3 and cannot be any larger.

1. MAXIMUM VALUE FOR THE SELECTION RATIO

The problem is, therefore, to maximize $A + B + d$, under the conditions:

$$A + b + d = 1 \quad (D.1)$$

$$-1 \leq a + B + d \leq 1 \quad (D.2)$$

$$-1 \leq a + b + d \leq 1 \quad (D.3)$$

This is solved simply as follows:

From (D.1) + (D.2) - (D.3), that is, from

$$1 = A + b + d = 1$$

$$-1 \leq a + B + d \leq 1$$

$$-1 \leq -(a+b+d) \leq 1$$

we have

$$-1 \leq A + B + d \leq 3 \quad (D.4)$$

The maximum selection ratio, therefore, has a value of 3.

2. VALUES OF WORD CURRENTS GIVING THE MAXIMUM SELECTION RATIO

The next problem is to seek the values of word current giving the maximum ratio of 3. When $A + B + d = 3$,

$$d = 3 - (A + B)$$

From (D.1) $b = 1 - (A + d) = B - 2$

From (D.2) $a \leq 1 - (B + d) = A - 2$

From (D.3) $a \geq -1 - (b + d) = A - 2$

Therefore,

$$a = A - 2 \quad (D.5)$$

Note that now $A + b + d = a + B + d = 1$ for half-selected cells and $a + b + d = -1$ for nonselected cells. Since A and B can be chosen arbitrarily, there is an infinite number of combinations of A and B.

It is reasonable to choose A and B to make the total drive power small. From this point of view, it is not advantageous to have a bias field applied to all cells, although its presence was assumed in the above discussion for generality. When there is no bias field, $d = 0$, so only either A or B can be chosen arbitrarily. Choosing A arbitrarily, then $B = 3 - A$, $a = A - 2$, $b = 1 - A$. Assuming that each word line has the same impedance and the total number of words is N, the sum of squares of each drive current may be considered to be a measure of drive power P.

Then,

$$P = A^2 + (3 - A)^2 + (\sqrt{N} - 1)(A - 2)^2 + \sqrt{N} - 1)(1 - A)^2 \quad (D.6)$$

The words are assumed to be arranged in a $\sqrt{N} \times \sqrt{N}$ matrix fashion. Transforming,

$$P = 2\sqrt{N}(A^2 - 3A) + 9 + 5\sqrt{N} - 5$$

$$P = 2\sqrt{N}\left(A - \frac{3}{2}\right)^2 + 4 + \frac{1}{2}\sqrt{N} \quad (D.7)$$

Thus the optimum values of drive currents giving the minimum drive power are;

$$A = \frac{3}{2},$$

$$B = 3 - A = \frac{3}{2},$$

$$a = A - 2 = -\frac{1}{2}$$

$$b = 1 - A = -\frac{1}{2}$$

The minimum drive power is $P_{\min} = 4 + \frac{1}{2}\sqrt{N}$.

Another choice is either $A = 1$ with $B = 2$, $a = 1$, $b = 0$, or $A = 2$ with $B = 1$, $a = 0$, $b = -1$, and $P = 4 + \sqrt{N}$ in either case. Since one of the drive currents is zero in these cases, the drive circuitry may be simpler.

Compared with the ordinary selection scheme requiring only 2 units of drive power with $A = B = 1$ and $a = b = 0$, the selection ratio of 3 is possible only at the cost of considerable power. This cost may

rarely be justifiable. Therefore, it is essential to improve memory materials so that writing can be done with the selection ratio of 2.

APPENDIX E

FACTORS INFLUENCING SWITCHING OF IDEAL FILMS

In addition to the fact that a magnetic thin film never switches exactly like the ideal single-domain model because of creep, incoherent rotation, and wall motion, there is also a variety of reasons why the film does not switch at the thresholds predicted by theory even if the film itself were the ideal one of the Stoner-Wohlfarth theory. The main factors are: nonuniformity of drive fields applied through strip lines, demagnetizing fields, film shape and edge effects, eddy currents in the drive lines, and capacitive coupling between the lines. Some of these factors were studied and the results are summarized below.

1. NONUNIFORMITY OF THE APPLIED FIELDS

Magnetic fields applied to thin films are usually expressed in terms of a scalar function of the currents in the drive conductors. This is appropriate for the case of uniform fields such as those produced by Helmholtz coils, very wide strip lines, or the circumferential field in a cylindrical film produced by the current in its round wire substrate. For fields produced by narrow strip lines, however, the use of a scalar function is often misleading, because the fields are not uniform over a memory cell. Two entirely different expressions for the strip-line fields can be obtained, depending upon whether the current distribution in the strip can be assumed uniform or not.

When a uniform current distribution is assumed throughout a thin strip line (width $2L$), the field $H_x(x, y)$, at the distance x from the center of the strip line (z -axis) in the plane parallel to the strip line at a distance y from the strip line, is calculated as follows. First the z -component of the vector potential is:

$$A_z = \frac{\mu}{4\pi} \int_{-\infty}^{\infty} \int_{-L}^L \frac{\frac{I}{2L}}{[(u-x)^2 + y^2 + z^2]^{1/2}} du dz \quad (\text{E. 1})$$

Then

$$\begin{aligned}
 H_x &= \frac{B_x}{\mu} = \frac{1}{\mu} \frac{\partial A_z}{\partial y} = \frac{I}{8\pi L} \int_{-\infty}^{\infty} \int_{-L}^L \frac{-y}{[(u-x)^2 + y^2 + z^2]^{3/2}} du dz \\
 &= -\frac{I}{4\pi L} \int_{-L}^L \frac{-y}{(u-x)^2 + y^2} du \\
 &= -\frac{I}{4\pi L} \left[\tan^{-1} \frac{u-x}{y} \right]_{-L}^L
 \end{aligned}$$

Disregarding the minus sign,

$$\begin{aligned}
 H_x(x, y) &= \frac{I}{4\pi L} \left[\pi - \tan^{-1} \frac{2yL}{L^2 - x^2 - y^2} \right] \quad \text{for } x^2 + y^2 \geq L^2 \\
 &= \frac{I}{4\pi L} \tan^{-1} \frac{2yL}{x^2 + y^2 - L^2} \quad \text{for } x^2 + y^2 \leq L^2
 \end{aligned} \quad (E. 2)$$

Since $A/m = 4\pi/1000$, the field in oersted is

$$H_x(x, y) = 2\pi \frac{I}{2L} \left[1 - \frac{1}{\pi} \tan^{-1} \frac{2yL}{L^2 - x^2 - y^2} \right] \quad \text{for } x^2 + y^2 \leq L^2$$

where L , x , and y are in mm., I is in amperes, and H is in oersteds.

If the ground plane is located at the distance d mm from the strip line, the field due to the ground plane is

$$H_g(x, y) = 2\pi \frac{I}{2L_1} \tan^{-1} \frac{2(2d-y)L}{x^2 + (2d-y)^2 - L^2} \quad \text{for } x^2 + (2d-y)^2 \geq L^2 \quad (E. 3)$$

The total field is, therefore,

$$H_x(x, y) = 2\pi \frac{I}{2L_1} \left[1 - \frac{1}{\pi} \tan^{-1} \frac{2yL_1}{L_1^2 - (x^2 + y^2)} + \frac{1}{\pi} \tan^{-1} \frac{2(2d-y)L_1}{x^2 + (2d-y)^2 - L_1^2} \right] \quad (E. 4)$$

assuming $x^2 + y^2 \leq L^2 \leq x^2 + (2d-y)^2$.

For $x = y = 0$ and $2d = L$,

$$H_x(0, 0) = 9.4 \times \frac{I}{2L_1} \text{ (oe)} \quad (\text{E. 5})$$

The above derivation assumes a constant current distribution. This assumption is valid for a sufficiently narrow strip line, but is not true for a wide line.

Without assuming a constant current density, H. J. Gray²¹ has shown that the magnetic field $H_x(x, y)$ in a shielded symmetrical strip line can be expressed as:

$$H_x(x, y) = - \frac{I}{4K(k)} \operatorname{Re} \frac{(\pi/2d) \operatorname{sech} \frac{\pi}{2d}(x + jy)}{\sqrt{k^2 - \tanh^2 \frac{\pi}{2d}(x + jy)}} \quad (\text{E. 6})$$

where I is the total current in the strip line, d is the distance between the strip line and the ground plane (another ground plane is assumed to be above the strip line at the same distance), $K(k)$ is the complete elliptic integral of the first kind with modulus k , $k = \tanh \frac{\pi L}{2d}$, and L is the half-width of the strip line.

The above expression may be used for the field near the strip line (for x, y small compared with d) in a nonsymmetric strip line with only one ground plane, though the actual field may be somewhat smaller, because it is not "compressed" by another ground plane.

Since $H_x(x, 0)$ is equal to the current density, $J(x, 0)$, per unit width of the strip line,

$$J(x, 0) = H_x(x, 0) = \frac{\pi I}{8dK(k)} \frac{1}{\sqrt{k^2 \cosh^2 \frac{\pi x}{2d} - \sinh^2 \frac{\pi x}{2d}}} \quad (\text{E. 7})$$

The fact that $J(L, 0) = \infty$ means that the field as well as the current density is infinitely large at the edges, $x = \pm L$. This is quite different from the constant-current distribution.

The center field $H_x(0, y)$ is

$$H_x(0, y) = \frac{\pi I}{8dK(k)} \frac{1}{\sqrt{k^2 \cosh^2 \frac{\pi y}{2d} + \sinh^2 \frac{\pi y}{2d}}} \quad (\text{E. 8})$$

It is noted that

$$H_x(0, 0) = \frac{\pi I}{8dK(k)k} \approx \frac{I}{2\pi L} \quad (\text{E. 9})$$

Assuming $L \ll d$, hence $k \approx \frac{\pi L}{2d}$ and $K(k) = \frac{\pi}{2}$, the edge field is

$$H_x(L, y) \approx \frac{\pi I}{8K(k)} \frac{1}{\sqrt{2\pi ykd}} \quad \text{for } y \ll d \quad (\text{E. 10})$$

Note that the various assumptions give radically different answers. Furthermore, for the geometries of practical significance no feasible analytical approaches appear to exist, except perhaps computer solutions.

2. DEMAGNETIZING FIELDS

Contrary to parts of the literature, the demagnetizing field in a flat thin film is a vector concept, in the sense that it varies from place to place in the film. It is determined by the difference of M at a point and the adjacent points, while M is determined in turn by the net field (applied fields plus the demagnetizing field) at those points. Thus the calculation of the demagnetizing field is very complicated.

When there is a magnetic charge q at $(l, 0)$, the x and y components of the demagnetizing field in c. g. s. units are

$$\left. \begin{aligned} H_{xd} &= -\frac{q}{r^2} \frac{l-x}{r} \\ H_{yd} &= -\frac{q}{r^2} \frac{y}{r} \end{aligned} \right\} \quad (\text{E. 11})$$

where $r^2 = (l-x)^2 + y^2$.

As a simple example, consider a single-domain film of length a , width b , and thickness t , with the easy axis along the a -edge. Let θ be the angle between the direction of the saturation magnetization, M_s , and the easy axis. The easy-axis component, H_{LD} , of the demagnetizing field at the center of the film is:

$$\begin{aligned}
 H_{LD} &= -2 \int_{-b/2}^{b/2} \frac{M_s t \frac{a}{2} \cos\theta}{\left[\left(\frac{a}{2}\right)^2 + y^2\right]^{3/2}} dy \\
 &= - \frac{8M_s tb}{a\sqrt{a^2 + b^2}} \cos\theta = -A \cos\theta
 \end{aligned} \tag{E. 12}$$

Similarly, the hard-axis component H_{TD} is:

$$H_{TD} = - \frac{8M_s ta}{b\sqrt{a^2 + b^2}} \sin\theta = -B \sin\theta \tag{E. 13}$$

If these fields are added to the applied fields, H_L , and H_T , the energy expression becomes

$$\begin{aligned}
 E &= \frac{1}{2} H_K M_s \sin^2\theta - [H_L - A \cos\theta] M_s \cos\theta - [H_T - B \sin\theta] M_s \sin\theta \\
 &= \frac{1}{2} [H_K - 2A + 2B] M_s \sin^2\theta - H_L M_s \cos\theta - H_T M_s \sin\theta + A M_s
 \end{aligned}$$

Thus the effective value of H_K , which we shall denote by H_K' , is

$$\begin{aligned}
 H_K' &= H_K - \frac{16 M_s tb}{a\sqrt{a^2 + b^2}} + \frac{16 M_s ta}{b\sqrt{a^2 + b^2}} \\
 &= H_K + \frac{16M_s t(a^2 - b^2)}{ab\sqrt{a^2 + b^2}}
 \end{aligned} \tag{E. 14}$$

It is interesting to note that H_K is unchanged when $a = b$.

It is also interesting to estimate the magnitude of the second term in H_K' . Suppose

$$a = 1 \text{ mm} = 10^{-1} \text{ cm (40 mils)}$$

$$b = 0.25 \text{ mm} = 2.5 \times 10^{-2} \text{ cm (10 mils)}$$

$$t = 500 \text{ \AA} = 5 \times 10^{-6} \text{ cm}$$

$$M_s = 10^4 \text{ gauss} = 8 \times 10^2 \text{ c. g. s. u.}$$

then

$$\frac{16M_s t(a^2 - b^2)}{ab\sqrt{a^2 + b^2}} = 2.6 \text{ oe}$$

If H_K is 3.0 oe, then the correction term is of comparable magnitude. This would indicate that the demagnetizing field is certainly too large to be neglected.

The foregoing discussion assumed that there were net magnetic charges $\pm M_s \cos\theta$ or $\pm M_s \sin\theta$ at the edges. Actually this is very unlikely from an energy point of view, because the demagnetizing field would then be infinitely large at the edges. It would be more realistic to assume that there is no magnetic charge at the edges. In this sense, the concept of a single domain is self-contradictory, because the single domain cannot exist without having free magnetic charges at the edges.

As an example of how the demagnetizing field may be calculated from a known distribution of magnetization, consider a strip of film of thickness t , which is infinitely long in the y direction. When there is a net line charge, $\Delta M(u_1)$ along $x = u_1$, and $\Delta M(-u_2)$ along $x = -u_2$, the demagnetizing field $\Delta H_D(x)$ in the x direction is:

$$\begin{aligned} \Delta H_D(x) &= \int_{-\infty}^{\infty} \frac{\Delta M(u_1) t (u_1 - x)}{[(u_1 - x)^2 + y^2]^{3/2}} dy - \int_{-\infty}^{\infty} \frac{\Delta M(-u_2) t (u_2 + x)}{[(u_2 + x)^2 + y^2]^{3/2}} dy \\ &= \frac{\Delta M(u_1) t}{u_1 - x} - \frac{\Delta M(-u_2) t}{u_2 + x} \end{aligned}$$

When $\Delta M(u)$ is known as a function of u , the total demagnetizing field

is calculated as
$$H_D(x) = \int_{-L}^L \Delta H(x) du$$

If we assume a form of $M(u)$ satisfying the following conditions:

- (1) $M(u) = M(-u)$ and $\Delta M(-u) = -\Delta M(u)$
- (2) $\Delta M(\pm L) = 0$ (no charge at the edges)
- (3) $M(0) = M_s$
- (4) $\Delta M(0) = 0$ (no charge at the center)

One such form of $M(u)$ is

$$\begin{aligned} M(u) &= M_s (L^3 - 3L^2u^2 + 2u^3)/L^3 && \text{for } 0 \leq u \leq L \\ &= M_s (L^3 - 3L^2u^2 - 2u^3)/L^3 && \text{for } -L \leq u \leq 0 \end{aligned}$$

and
$$\begin{aligned} \Delta M(u) &= 6 M_s u(u-L) \Delta u/L^3 && \text{for } 0 \leq u \leq L \\ &= -6 M_s u(u+L) \Delta u/L^3 && \text{for } -L \leq u \leq 0 \end{aligned}$$

Then,

$$\begin{aligned} H_D(x) &= \frac{6M_s d}{L^3} \left[\int_0^L \frac{u(u-L)}{u-x} du + \int_{-L}^0 \frac{u(u+L)}{u+x} du \right] \\ &= -\frac{6M_s d}{L^3} \left[1 + \frac{x(L-x)}{L^2} \log \left| \frac{L-x}{x} \right| - \frac{x(L+x)}{L^2} \log \left| \frac{L+x}{x} \right| \right] \end{aligned}$$

It is noted that

$$\begin{aligned} H_D(x) &= H_D(-x) \\ H_D(0) &= -6 M_s d/L^3 \\ H_D(\pm \frac{1}{2} L) &= 0.18 H_D(0) \\ H_D(\pm L) &= (1-2 \log 2) H_D(0) = -0.38 H_D(0) \end{aligned}$$

The demagnetizing field becomes zero at x slightly larger than $L/2$ and changes sign for greater values of x . This can be interpreted from Fig. 23. The fact that the demagnetizing field can be in the same direction as the magnetization has also been pointed out by H. J. Kump.²²

A more elaborate one-dimensional analysis using a computer has been reported by H. J. Kump,²² who has used the single-domain model equations to determine ΔM from the total field (demagnetizing field plus applied field by a narrow strip line). The boundary condition is that the total net field at the edges is zero, that is, the demagnetizing field is equal to the applied field in magnitude, but is opposite in sign at the edges. The results show that it is difficult to orient the entire (or nearly entire) film at 90° from the easy axis because of the

nonuniformity of the applied field and the large demagnetizing field. Here the easy axis is assumed to be in the direction of the strip.

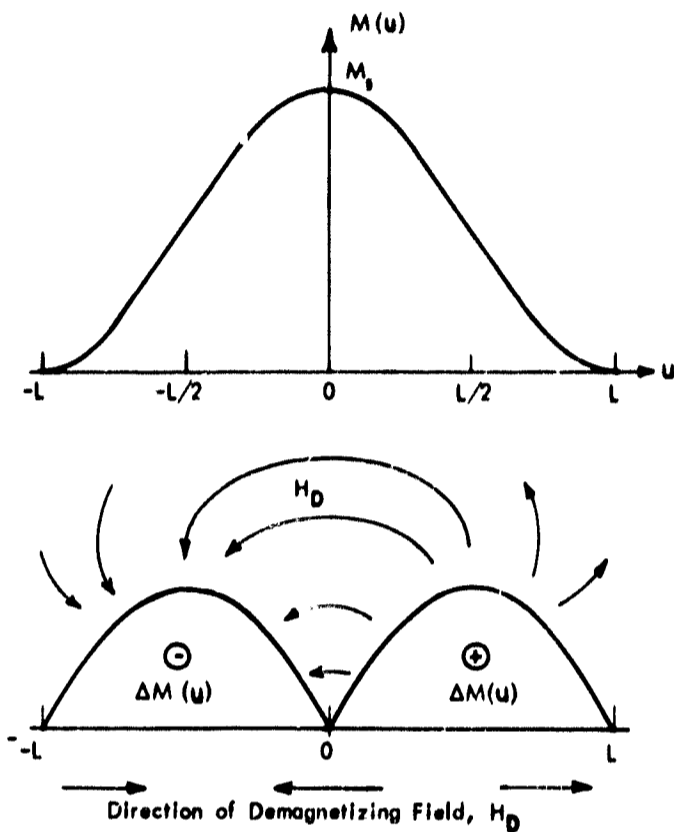


Fig. 23 Model for Magnetization and Demagnetizing Field Distributions

To see the effect of the demagnetizing field on switching, it is necessary to consider two orthogonal fields and the analysis must be done on a two-dimensional basis. It is convenient to assume that the film consists of a number of tiny rectangular single domains, with the easy axis in the x direction. The demagnetizing field $H_D(x, y)$ at any point (x, y) can then be calculated by counting the contribution from each and every domain.

It would be interesting to solve this problem with the aid of a computer and to see how much area of the film switches at a certain level of applied fields and to determine the shape of that area. Actually, however, this is a two-dimensional problem and its solution would require a very long computer time. Moreover, the assumption that the single domain theory is applicable to each individual cell might not be realistic especially where switching is involved. For these reasons, a computer solution was not attempted.

3. EDDY CURRENT

The eddy current is induced in a metal by a changing magnetic field. The total eddy current in a metal sheet of thickness t , width a , length l , as shown in Fig. 24 can be shown to be²³

$$i = \frac{t^2}{8} \frac{l}{\rho} \frac{dB}{dt} \quad \text{for } a \gg t$$

where ρ is the specific resistivity.

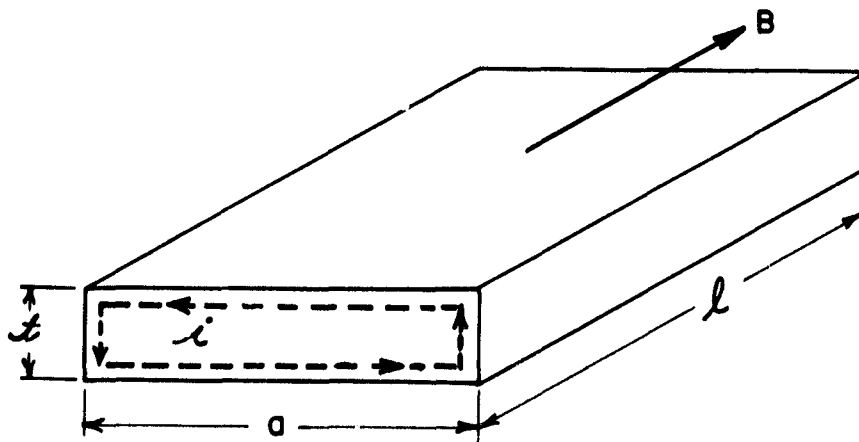


Fig. 24 Eddy Current Pattern in a Conductor

There are two kinds of magnetic fields present in a drive conductor. One is the field produced by the other drive line and the other is the piercing flux from the film. The eddy current due to the former acts to shield the magnetic field and thus distort it. The eddy current due to the latter acts as a damping torque against flux change. Thus, it tends to return the switched magnetization to its previous state and therefore slows down switching. The effective H_k is increased by this damping effect. When a metal substrate is used, the eddy current induced in the substrate must also be taken into account, because it also opposes any change in magnetization.²⁴ There is also speculation that the magnetic thin film has a metallic behavior in supporting eddy currents over its surface, thus severely distorting the field configuration.

A detailed analysis of the eddy current effect is very complicated and it is difficult to get even an approximate expression. T. A. Smay²⁵ has attempted an approximate analysis but it is difficult to justify the assumptions.

As for actually observed effects of eddy currents, there are conflicting reports. It is J. S. Eggenberger's²⁶ conclusion that the rotation mode of switching is difficult to achieve in a strip line configuration of reasonable size (1 mm width or so). According to J. G. Edwards,²⁴ eddy current effects are not significant in 0.5 mm (20 mil) wide strip lines, though the effects are appreciable in lines more than 1 mm (40 mils) wide.

APPENDIX F

RADIO-FREQUENCY DRIVE-LINE AND SENSE CIRCUITRY

The drive-line and sense circuitry is quite conventional, with little attempt being made to minimize the number of components used. The drive and sense circuitry is shown in schematic form in Fig. 25.

The fundamental 10 MHz signal is obtained from a Colpitts oscillator. This signal is converted to 40 MHz by means of a transformer coupled class C amplifier. The 40 MHz signal is then amplified and fed to the drive-lines by several tuned collector stages. The 20 MHz signal is similarly converted from the 10 MHz signal by means of a class C amplifier. Prior to conversion to 20 MHz the 10 MHz signal is converted to a square wave from which the trigger pulse necessary to operate a monostable multivibrator is derived. The on-time of this multivibrator is variable so that the timing and therefore the phase of the subsequent class C, 10 MHz to 20 MHz, amplifier is adjustable. The final output amplifier consists of several tuned-collector stages. The 20 MHz and 40 MHz outputs are capacitively coupled to the drive lines. The 20 MHz and 40 MHz amplifiers are capable of providing 500 mA and 200 mA peak current amplitudes respectively. Measurements of the drive-line impedances using a Hewlett-Packard 1415A Time Domain Reflectometer indicate average impedances in the range 60 ohms to 80 ohms, in agreement with calculated values.²⁷

The sense amplifier has four tuned-collector stages, preceded by an L-C filter having a series and a shunt section. The series section is a 60 MHz-pass and 20 MHz-block, while the shunt section is a 60 MHz-block and 40 MHz-pass. The transfer function of the filter has the form

$$f(s) = \frac{(s^2 + \omega_0^2)(s^2 + 4\omega_0^2)}{a s^2 (s^2 + 9\omega_0^2) + (s^2 + \omega_0^2)(s^2 + 4\omega_0^2)}$$

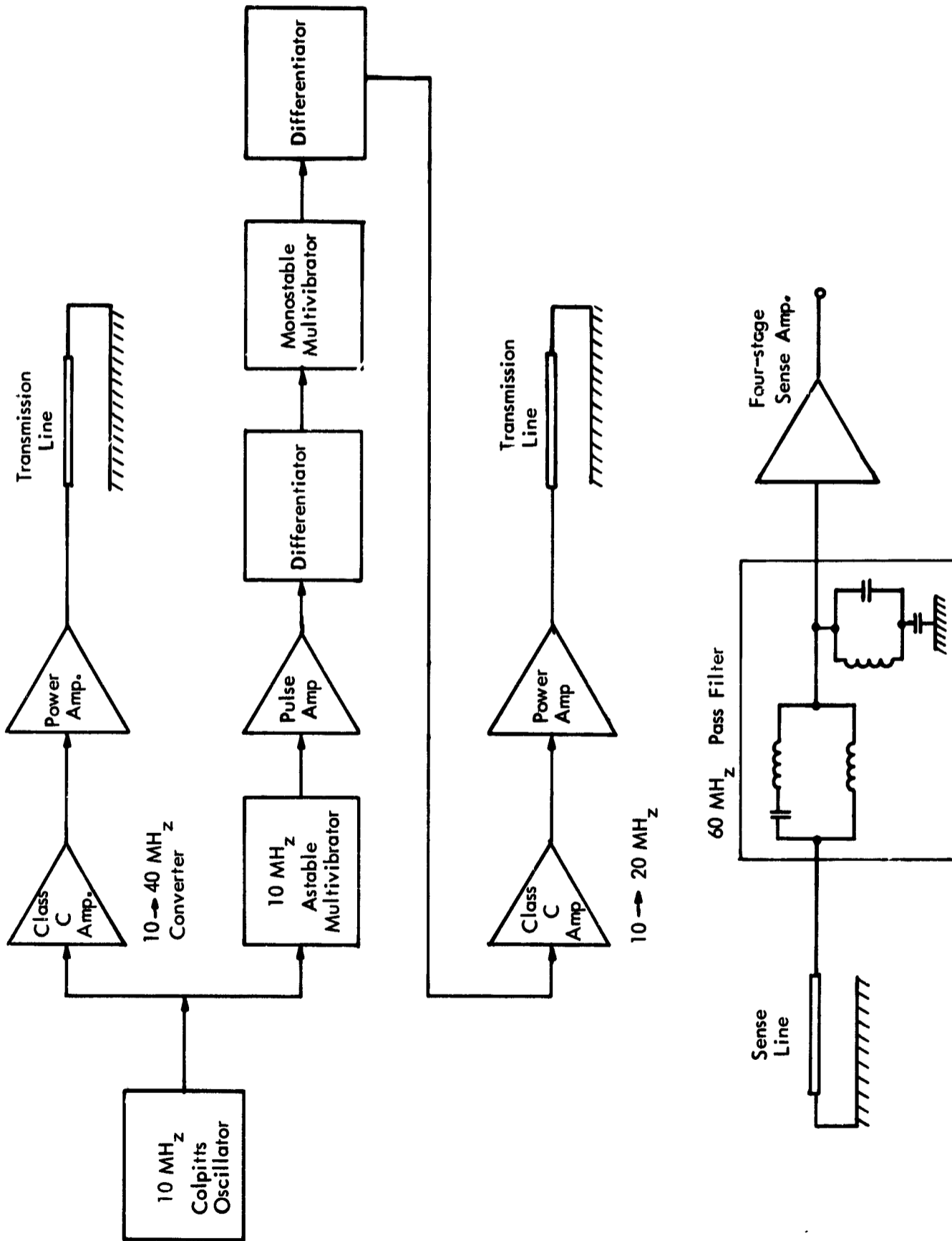


Fig. 25 Radio-Frequency Drive and Sense Circuitry Block Diagram

REFERENCES

1. Widrow, B., "Radio-Frequency Nondestructive Readout for Magnetic-Core Memories," IRE Transactions on Electronic Computers, Vol. EC-3, December, 1965, pp. 12-15.
2. Hoper, J. H., "NDRO Magnetic Film Memory Mode Using Creep and Boundary Displacement Switching," Journal of Applied Physics, Vol. 35, No. 3 (Part 2), 1964, p. 762.
3. Bader, C. J., and Ellis, D. M., "Instrument for Observation of Magnetization Vector Position in Thin-Magnetic Films," Review of Scientific Instruments, Vol. 33, No. 12, 1962, p. 1429.
4. Fuller, H. W., et al., "System and Fabrication Techniques for a Solid-State Random-Access Mass-Memory," IEEE Transactions on Magnetics, Vol. MAG-1, 1965, pp. 21-25.
5. Webber, R. J., et al., "Efficiency of High-Frequency Mixing in a Permalloy Toroid," Journal of Applied Physics, Vol. 33, 1962, p. 2026.
6. Zappe, H. H., "The Microprobe Tester -- An Instrument for the Local Evaluation of Magnetic Films," Journal of Applied Physics, Vol. 38, No. 3, 1967, p. 1434.
7. Soohoo, R. F., Magnetic Thin Films, Harper and Row, New York, 1965, p. 241.
8. Crowther, T. S., M.I.T. Lincoln Laboratory Group Report No. 51-2 (1959), revised 30 March 1960.
9. Smith, D. O., "Anisotropy in Permalloy Films," Journal of Applied Physics, Supplement to Vol. 30, April, 1959, p. 2648.
10. Feldtkeller, E., and Stein, K. U., "Improved Magnetic Film Elements for Memory Application," INTERMAG Conference Proceedings, Session 8.4, 1965.
11. Néel, L., Comptes Rendus, Vol. 255, 1962, p. 1676.
12. Bruyère, J. C., Massenet, O., Montmory, R., and Néel, L., IEEE Transactions on Magnetics, Vol. MAG-1, 1965, p. 10.
13. Middelhoek, S., "Domain-Wall Structures in Magnetic Double Films," Journal of Applied Physics, Vol. 37, No. 3, 1966, p. 1276.
14. Bruyère, J. C., et al., IEEE Transactions on Magnetics, Vol. MAG-1, 1965, p. 174.

REFERENCES (Contd.)

15. Feldtkeller, E., "Coupled Walls in Multilayer Films," Journal of Applied Physics, Vol. 39, 1968, p. 1181.
16. Stein, K. U., "Impulsuntersuchungen an magnetischen Mehrfachschichten und an Nickeleisenschichten mit eindiffundierten Kupfer," Zeitschrift Angewandte Physik, Vol. 21, 1966, p. 400.
17. Slutz, D. R., "Creep Writing in a NDRO Thin-Film Memory," S. M. Thesis, Massachusetts Institute of Technology, Department of Electrical Engineering, August, 1965.
18. Middelhoek, S., and Wild, D., "Review of Wall-Creeping in Thin Magnetic Films," IBM Journal of Research and Development, Vol. 11, January, 1967, pp. 93-105.
19. Hagedorn, F. B., "Exchange Anisotropy in Oxidized Permalloy Thin Films at Low Temperatures," Journal of Applied Physics, Vol. 38, No. 9, 1967, p. 3641.
20. CRC Mathematical Tables, 13th Edition, 1964, p. 366.
21. Gray, H. J., "Fields in Strip-Lines for Film Memory Application," IEEE Transactions on Electronic Computers, Vol. EC-13, 1964, p. 576.
22. Kump, H. J., "Demagnetization of Flat Uniaxial Films under Hard Direction Drive," IBM Journal of Research and Development, Vol. 9, 1965, p. 118.
23. Soohoo, R. F., Magnetic Thin Films, Harper and Row, New York, 1965, p. 137.
24. Edwards, J. G., "Investigation of Some High-Speed Switching Properties of Magnetic Films," Proceedings of the Institution of Electrical Engineers, (London), Vol. 112, No. 6, 1965, pp. 1081-1090.
25. Smay, T. A., "Energy Transfer Properties of Thin Magnetic Film Logical Elements," Ph. D. Thesis, Iowa State University, 1962.
26. Eggenberger, J. S., "Influence of Nearby Conductors on Thin-Film Switching," Journal of Applied Physics, Supplement to Vol. 31, No. 5, 1960, p. 287S.
27. Wheeler, H. A., "Transmission-line Properties of Parallel Strips Separated by a Dielectric Sheet," IEEE Transactions on Microwave Theory and Techniques, Vol. MTT-13, No. 2, March, 1965, p. 172.

PREVIOUS INTERIM REPORTING OF THE
WORK DESCRIBED IN THIS REPORT

The following four Interim Technical Documentary Reports prepared by the Electronic Systems Laboratory under Contract AF-33(657)-11311 (MIT Project DSR 79891) for the Air Force Avionics Laboratory, Wright-Patterson Air Force Base, Ohio, describe the initiation and initial phases of the coincident radio-frequency readout investigations:

ESL-IR-190,	January 1964,	pp. 32-38
ESL-IR-197,	April 1964,	pp. 31-42
ESL-IR-208,	July 1964,	pp. 23-40
ESL-IR-217,	October 1964,	pp. 40-49

Starting in 1965, the work was continued under NASA Grant NsG-496 (Part), MIT Projects 9948 and 76152, and reported in the following Status Reports issued by the Electronic Systems Laboratory under this grant:

ESL-SR-256 (Part II),	December 1965,	pp. 5-28
ESL-SR-274 (Part II),	June 1966,	pp. 2-9
ESL-SR-298 (Part II),	January 1967,	pp. 13-16